Identification of a Hypoxia-induced Inflammatory Cell Death Pathway

Abhishek Bhardwaj[1,5*], Maria Antonelli[1,2], Beatrix Ueberheide[1,2,3,4], Benjamin G. Neel[1]

[1] Laura and Isaac Perlmutter Cancer Center, New York University Grossman School of Medicine, NYU Langone Health, New York, NY, USA
[2]Proteomics Laboratory, Division of Advanced Research Technologies, New York University Grossman School of Medicine, New York, NY, USA
[3]Department of Biochemistry and Molecular Pharmacology, New York University Grossman School of Medicine, New York, NY, USA
[4]Department of Neurology, New York University Grossman School of Medicine, New York, NY, USA
[5]Lead Contact

*Correspondence: abhishek.bhardwaj@nyulangone.org (A.B.)

Summary

Hypoxic cancer cells resist many anti-neoplastic therapies and can seed recurrence. We found previously that PTP1B deficiency promotes HER2+ breast cancer cell death in hypoxia by activating RNF213, an ~600kDa protein containing AAA-ATPase domains and two ubiquitin ligase domains (RING and RZ), which is implicated in Moyamoya disease (MMD). Here we report that PTP1B and ABL1/2 reciprocally control RNF213 phosphorylation on tyrosine-1275. This phosphorylation promotes RNF213 oligomerization and RZ domain activation. The RZ domain ubiquitylates CYLD/SPATA2, and together with the LUBAC complex, induces their degradation. Decreased CYLD/SPATA2 levels cause NF-κB activation, which together with hypoxia-induced ER-stress triggers pyroptosis. Mutagenesis experiments show that the RING domain negatively regulates the RZ domain, and RING mutants, including MMD alleles, catalyze LUBAC-independent CYLD/SPATA2 degradation. Our results identify an inflammatory cell death pathway that kills hypoxic tumors, reveal new insights into RNF213 regulation, and have important implications for MMD, atherosclerosis, and inflammatory disorder pathogenesis.

Keywords: RNF213; PTP1B; CYLD; LUBAC; NF-κB; Hypoxia; Inflammation; ER-stress; Pyroptosis; MMD.

Introduction

Most tumors have hypoxic or anoxic areas.[1] In response, cancer cells adapt to limited oxygen in the tumor microenviroment (TME) by successively activating several signaling pathways. In normoxia, the transcription factors HIF1α and HIF2α (hereafter "HIF") are hydroxylated by oxygen-dependent prolyl hydroxylases (PHD 1-3), bound by the Van Hippel Lindau tumor suppressor gene product (VHL), and targeted for ubiquitylation and proteosomal degradation.[2] PHD enzymes are inhibited in low oxygen, resulting in HIF stabilization and induction of hypoxia response genes. More severe hypoxia ($\leq$1% O_2) triggers the AMP-dependent kinase (AMPK) and endoplasmic reticulum (ER) stress pathways, which evoke distinct adaptive responses.[3,4] The activity of NF-κB, a key transcription factor controlling inflammation and innate immunity, also increases in hypoxia via (an) incompletely defined mechanism(s) that include(s) decreased PHD regulation of NF-κB pathway signaling components.[5] Conversely, NF-κB is required for basal *HIF1alpha* expression, and thus directly and indirectly regulates the transcriptome of hypoxic cells.[6] The complex interplay between HIF-induced, metabolic (AMPK), integrated stress response (ER stress), and inflammatory/innate immune (NF-κB)[7,8] pathways helps determine cancer cell sensitivity to conventional (chemoradiation) and targeted therapy,[3] as well as whether tumor cell death evoked by antineoplastic therapies is "sterile" or immunogenic.[9-11]

The protein-tyrosine phosphatase PTP1B (encoded by *PTPN1*) resides on the cytosolic surface of the endoplasmic reticulum (ER), where it dephosphorylates incoming receptor tyrosine kinases (RTKs) and cytokine receptors.[12,13] Best known as a negative regulator of insulin and leptin signaling,[14-17] PTP1B is also required for *Neu* (encoding rodent HER2)-induced breast cancer in mice.[18,19] Moreover, *PTPN1* is amplified (~5%) and overexpressed (~72%) in human cancer.[20,21] Previously, we reported that PTP1B deficiency or inhibition increases the death of HER2+ breast cancer cells maintained at $\leq$1% O_2 without altering the HIF, ER stress, or AMPK pathways.[22] Instead, hypoxia hypersensitivity required RNF213, a large (~600 kDa) protein with AAA-ATPase and E3 ligase domains. PTP1B deficiency/inhibition promoted an increase in RNF213-dependent global ubiquitylation, and RNF213 was tyrosine phosphorylated and appeared to be a PTP1B substrate. However, key details, including how PTP1B regulates RNF213 and the mechanism and type of RNF213-dependent cell death, remained unclear.

Single nucleotide polymorphisms (SNPs) in *RNF213* are associated with Moyamoya disease (MMD), a rare syndrome characterized by precocious carotid artery stenosis and stroke, often in teenagers or young adults.[23-25] RNF213 features six AAA-ATPase modules, two of which are active, a RING E3 ligase domain, a recently discovered "RZ" E3 domain, and large unstructured regions.[26-30] In an AAA-ATPase- and ISG15-dependent manner, RNF213 can oligomerize into a hexameric, ~3.6mDa complex.[26,28] RNF213 localizes on lipid droplets[31] (also dependent on AAA-ATPase activity/ISG15) and is required for lysophosphatidic acid (LPA)-induced cell death *in vitro*.[32] Transfection studies implicate RNF213 in NF-κB signaling,[30,32] and recently, the RNF213 RZ domain was reported to ubiquitylate lipid A of Salmonella.[29] In concert, these findings suggest roles for RNF213 in lipoxicity and inflammation, both potentially relevant for MMD pathogenesis as well as cancer and other diseases. However, the most highly penetrant MMD SNPs affect the RNF213 RING, not the RZ domain,[27,30,33] leaving the detailed

molecular pathogenesis of this disease and its relationship, if any, to hypoxia hypersensitivity in PTP1B-deficient/inhibited breast cancer cells obscure.

We found that ABL1/2 phosphorylate, whereas PTP1B dephosphorylates, RNF213 on tyrosine 1275 (Y1275) in breast cancer cells. Phosphorylation of this site promotes RNF213 oligomerization and activation of its E3 ligase activity. We identify the CYLD-SPATA2 complex, a major negative regulator of NF-κB activation, as an RNF213 substrate critical for hypoxia-induced cell death. The RZ domain is required for CYLD-SPATA2 ubiquitylation/degradation, while the RING domain restrains RZ activity. Wild type RNF213 requires the LUBAC complex for effective CYLD-SPATA2 degradation, but RNF213 RING mutants, including highly penetrant SNPs associated with MMD, bypass this requirement. Increased RNF213 activity, caused by PTP1B deficiency/inhibition or RNF213 RING mutations, drives CYLD/SPATA2 ubiquitylation and degradation and increases NF-κB activity, priming cells for pyroptosis via the NLRP3 inflammasome. Concomitantly, hypoxia-induced ER stress delivers the "second signal" triggering cancer cell death. Deletion of SPATA2 phenocopies the effects of *PTPN1* deletion on tumorigenesis by HER2+ breast cancer cells. Our results have implications for the mechanism of action and potential uses of dual inhibitors of PTP1B/TC-PTP (*PTPN2*),[34] now in clinical trials for various cancers, as well as for the pathogenesis of MMD and other steno-occlusive disorders.

Results

Y1275 phosphorylation of RNF213 is regulated by PTP1B/ABL, which promotes RNF213 oligomerization.

We have reported that HER2+ breast cancer cells with *PTPN1* knockdown or treated with a PTP1B inhibitor are hypersensitive to hypoxia.[22] By studying an expanded panel of breast cancer cell lines, we found that hypoxia hypersensitivity is not limited to the HER2+ subtype; treatment with the allosteric PTP1B inhibitor claramine also caused hypoxia hypersensitivity in several ER+ and triple negative (TNBC) breast cancer lines (Figure S1A). Hence, PTP1B is more general regulator of the hypoxia response, at least in breast cancer cells and possibly in other malignancies.

We also found previously that RNF213 is tyrosine phosphorylated in HER2+ breast cancer cells and interacts with PTP1B. "Substrate-trapping" mutants of PTP1B show increased RNF213 binding, and this interaction is competed by the active site PTP inhibitor sodium orthovanadate, which suggested that RNF213 is a PTP1B substrate.[22] However, RNF213 tyrosine phosphorylation is not increased in PTP1B-inhibited/deficient HER2+ breast cancer cells, indicating that only select sites are PTP1B targets. We generated an RNF213-TurboID fusion protein with the goal of identifying RNF213 binding partners by proximity ligation[35] (see below), labelled interacting proteins with biotin, enriched these proteins on streptavidin beads, performed on-bead tryptic digestion, and analyzed the peptide mixture by mass spectrometry (MS). This analysis revealed evidence of RNF213 phosphorylation on residue Y1275 (Table S1, Figure S1B).

To ask whether this phosphorylation is relevant for RNF213/PTP1B interaction, we used CRISPR/Cas9 to generate *RNF213*-knockout (KO) BT474 cells and retroviral gene transduction to introduce *PTPN1* or non-targeting (Control) shRNAs. We transduced these cells with an lentivirus expressing hemaglutinin (HA) tagged-mouse *Ptpn1*$^{D/A}$, which encodes the substrate-trapping mutant PTP1B^{D181A} (HA-PTP1B$^{D/A}$). The resultant lines were transfected with expression vectors for 3x-FLAG-*RNF213* or 3x-FLAG-*RNF213*^{Y1275F}. Immunoprecipitation (IP) of HA-PTP1B$^{D/A}$ resulted in recovery of 3x-FLAG-RNF213. Much less 3x-FLAG-RNF213^{Y1275F} co-immunoprecipitated (Figure 1A, right), even though it was expressed at comparable levels to wild-type RNF213 (Figure 1A, left). Similar results were obtained from analogous experiments with AU565-derived cell lines (Figure S1C). Tyrosine phosphorylation of 3x-FLAG-RNF213^{Y1275F} was reduced compared with that of 3x-FLAG-RNF213, but to a lesser extent (~40%) than the near total decrease in 3x-FLAG-RNF213^{Y1275F} recovery in HA-mPTP1B$^{D/A}$ immunoprecipitates (Compare Fig,1A and 1B and Fig. S1C and S1D). These data suggest that additional tyrosine phosphorylation sites exist in RNF213 that are not detected by MS or that new sites are generated in RNF213^{Y1275F}. Regardless, our results indicate that RNF213-Y1275 is a specific site for PTP1B-catalyzed dephosphorylation.

PTP1B deficiency/inhibition markedly increases overall cellular ubiquitylation, dependent on RNF213.[22] Y1275 is distant from the RING or RZ domains in the monomeric RNF213 structure,[26] arguing against direct regulation. We therefore tested the hypothesis that phosphorylation affects RNF213 oligomerization by co-transfecting expression vectors for 3x-FLAG-*RNF213* or 3x-FLAG-*RNF213*^{Y1275F} and *GFP-RNF213* and performing anti-FLAG

immunoprecipitations. Notably, recovery of GFP-RNF213 in 3x-FLAG-RNF213^{Y1275F} immunprecipitates was impaired in BT474 (Figure 1D) and AU565 cells (Figure S1E).

We next sought the kinase(s) that phosphorylate(s) RNF213-Y1275. ABL family kinase inhibitors (dasatinib, asciminib) abrogated the hypoxia hypersensitivity of BT474 *PTPN1*-KO cells and SKBR3 *PTPN1*-KO cells (Figure 1D; Figure S2A). Dasatanib treatment (compared to treatment with DMSO vehicle alone) also dramatically reduced the recovery of RNF213 in PTP1B trapping mutant immunoprecipates from these cells (Figure 1E, right; Figure S2B) and reduced overall RNF213 tyrosine phosphorylation to an extent similar to that caused by Y1275F mutation (Figure 1F; Figure S2C). We therefore asked whether ABL1 phosphorylates RNF213 *in vitro*. We immunopurified FLAG 3x-FLAG-RNF213 and 3x-FLAG-RNF213^{Y1275F} (Figure S2D), incubated them with recombinant, His-tagged ABL1, and found that His-ABL1 phosphorylated WT-RNF213, but not RNF213^{Y1275F}, in a ABL1-concentration and time -dependent manner (Figure 1G; Figure S2E). Furthermore, *ABL1/2* siRNA-treated cells were resistant to hypoxia hypersensitivity induced by PTP1B deficiency (Figure 1H). Similar results were observed using parental and *PTPN1*-KO MDAMB361 cells (Figure S2F). We conclude that RNF213 Y1275 phosphorylation is regulated by PTP1B and ABL1/2, and phosphorylation of this site promotes RNF213 oligomerization and hypoxia hypersensitivity.

RNF213 interacts with CYLD and SPATA2

To begin to understand how RNF213 regulates hypoxia sensitivity, we identified RNF213-interacting proteins (Figure 2A). TurboID-*RNF213* ("N-Turbo"), *RNF213*-TurboID ("C-Turbo"), or TurboID alone (Control Turbo) were recombined into HeLa FlpIn-TRex *RNF213*-KO cells. These cells were labelled with biotin for 10 min., and biotinylated proteins were recovered on streptavidin, digested with trypsin, and analyzed by MS (Figure 2A). Proteins were ranked as potential binding partners by using the SAINT express algorithm.[36] Immunoblotting (Figure S3A) and silver staining (Figure S3B) confirmed that similar amounts of each sample were submitted for analysis. Relatively few proteins were labelled by N-Turbo (Figure S3C). By contrast, C-Turbo labelled PTP1B (PTPN1) and USP15 (blue-colored arrows), previously reported to interact with RNF213,[22,37] as well as several new proteins were significantly enriched over the control sample (Figure 2B, Table S2). Among the other top candidates were the major K63-deubiquitinase and NF-κB regulator CYLD and its interacting protein SPATA2 (Figure 2B, orange-colored arrows). RNF213/CYLD interaction was recently reported by another group, although its biological significance was not determined.[38] Other top C-Turbo interactors included proteins involved in VEGF signaling, which is induced in hypoxia (FLII, MYOF),[39,40] inflammation and atherosclerosis (MAP4K4, SPTLC1),[41,42] lipotoxicity (SPTLC1, ALDH1B1),[43,44] ischemia response (CPEB4),[45] and stroke (SARS2).[46] Top N-Turbo interactors included CYP51A1, which plays a crucial role in cholesterol metabolism and atherosclerosis.[47] Pathway analysis suggests involvement of RNF213 in K63-linked deubiquitylation, cytokine (including interferon)-mediated signaling, innate immunity, necroptotic cell death, and cytoskeletal regulation (Figure S3D and S3E).

Given their role in NF-κB response, inflammation, and innate immunity, we focused on the CYLD/SPATA2 interaction with RNF213. Immunoblotting confirmed the interaction of C-Turbo, but not Turbo alone, with CYLD, SPATA2, and, as expected, PTP1B; neither Turbo protein interacted with ERK2, which served as a control for non-specific biotinylation (Figure 2C). CYLD

and SPATA2 also co-immunopreciptated with 3x-FLAG-RNF213 expressed by transient transfection of BT474-*RNF213*-KO-sh*PTPN1* cells (Figure 2D). We next used CRISPR/Cas9 technology and two independent sgRNAs to delete each gene in BT474 and BT474 *PTPN1*-KO cells. Remarkably, *CYLD*-KO or *SPATA2*-KO sensitized BT474 cells to hypoxia even more than *PTPN1*-KO alone (Figure 2E). Similar results were obtained when analogous SKBR3-derived cell lines were studied (Figure S4A and S4B). Hence, RNF213 interacts with CYLD and SPATA2, and CYLD and SPATA2 (and, most likely, the CYLD/SPATA2 complex) prevent hypoxia hypersensitivity in breast cancer cell lines.

RNF213 uses its RZ domain to ubiquitylate CYLD and SPATA2

To test whether CYLD and SPATA2 are RNF213 substrates, we co-expressed ALFA-tagged SPATA2 or CYLD and HA-Ubiquitin (HA-UB) in parental or *RNF213*-KO BT474 cells, and treated these cells with claramine (10μM) or vehicle (Figure 3A). As expected, co-transfection of UB resulted in an increase in HA-reactive species, which were enhanced further in ALFA-CYLD- or ALFA-SPATA2-expressing cells. Comporting with our previous report,[22] claramine treatment led to an increase in overall ubiquitylation (Figure 3A, left). Recovery of each ALFA-tagged protein, followed by anti-HA immunoblotting, revealed RNF213-dependent ubiquitylation of CYLD and SPATA2, which was enhanced by PTP1B inhibition (Figure 3A, right). Analogous results were obtained using AU565 cells (Figure S4C).

We purified 3xFLAG-tagged RNF213 and various RNF213 mutants from HeLa FlpIn-TRex *RNF213*-KO cells (Figure S4D top, bottom), and assessed the ability of each protein to ubiquitylate CYLD and SPATA2 *in vitro* using UBE1 as the E1 enzyme and UBE2L3 as the E2. Consistent with our transfection studies, SPATA2 and CYLD, when tested alone or in equimolar concentrations, were ubiquitinated by 3xFLAG-RNF213 (Figure 3B). As noted above, RNF213 has two potential ubiquitin ligase domains (RING, RZ; catalytic histidines indicated in the cartoon in Fig. 3C). There was no significant ubiquitylation of CYLD or SPATA2 by an RZ mutant ("RZ-dead") form of RNF213 ($RNF213^{H4509A}$, Figure 3D). Surprisingly, however, CYLD or SPATA2 ubiquitylation was *increased* when RING mutant RNF213 ($RNF213^{H4014A}$, "RING-dead") was assayed (Figure 3E). Based on these results, we hypothesized that the RING negatively regulates the RZ domain. We therefore compared the ubiquitylation activity of WT RNF213 and $RNF213^{H4014A/H4509A}$ (RING/RZ-dead). Consistent with our hypothesis RING/RZ-dead RNF213 was unable to ubiquitylate CYLD/SPATA2 (Figure 3F). Therefore, RNF213 is an E3-ubiquitin ligase for CYLD and SPATA2, their ubiquitylation is catalyzed by the RZ domain, and the RING can restrain RZ activity. Furthermore, RING-dead (or RING-impaired) mutations are RNF213 RZ gain-of-function mutants; notably, highly penetrant MMD SNPs map to the RING domain.

These findings were surprising, because we reported earlier that RING-dead RNF213 or highly penetrant MMD SNPs *decrease* global ubiquitylation in HeLa or 293T cells and appear to act as dominant negative alleles. By contrast, our new data suggest that RING-dead RNF123 is an RZ gain-of-function mutation, which might be expected to *increase* global ubiquitylation. In an attempt to resolve this apparent discrepancy, we co-expressed 3xFLAG-RNF213 or RNF213 mutants with HA-Ubiquitin (HA-UB) in HeLa Flp-In-TRex *RNF213*-KO cells (Figure S4E) and subjected these cells to normoxia or hypoxia (0.1% O_2 for 24 hours). Consistent with our previous report, we observed a sharp decrease in *global* ubiquitylation with the RING-dead mutant; however, global ubiquitylation also was decreased in cells expressing RZ-dead or RING-

and RZ-dead RNF213. Similar results were observed in experiments with BT474 *RNF213*-KO cells reconstituted with *RNF213* or various *RNF213* mutants (Figure S4F). These data suggest that RING and RZ domain each have unique substrates, and that negative regulation of the RZ domain by the RING is probably substrate-specific. Alternatively, the RZ domain could regulate targets that, in concert, perturb global ubiquitylation.

The RNF213 RZ and ATPase domains promote hypoxia hypersensitivity via degradation of SPATA2 and CYLD

To determine which RNF213 domains are required for hypoxia hypersensitivity, we reconstituted BT474 *RNF213*-KO (and AU565-*RNF213*-KO) cells with WT *RNF213*, *RNF213*^{Y1275F}, *RNF213*^{K2775A} (second AAA-ATPase domain mutant), *RNF213*^{H4014A} (RING-dead), *RNF213*^{H4509A} (RZ-dead), *RNF213*$^{H4014A/H4509A}$ (RING/RZ-dead) or *RNF213*$^{K2775A/H4014A}$ (ATPase/RZ-dead), as indicated in Figure 4A. We also used CRISPR/Cas9 to generate *PTPN1*-KO pools of each cell line. The resultant cell lines/pools were subjected to hypoxia, and lysates were analyzed by immunoblotting. As expected, WT RNF213, but not RNF213^{Y1275F}, promoted CYLD and, to a lesser extent, SPATA2 degradation in BT474 (Figure 4B) and AU565 cells (Figure S5A). Also as expected, degradation was increased by PTP1B deficiency. RZ-dead or RING/RZ-dead RNF213 were unable to promote CYLD or SPATA2 degradation, whereas compared with WT RNF213, the RING-dead mutant enhanced degradation (Figure 4C; Figure S5B), especially in the *PTPN1*-KO background. Previous work showed that RNF213 ATPase activity is required for RZ domain-mediated ubiquitin ligase activity[29]. Given our finding that RING-dead mutations show RZ domain gain-of function, we hypothesized that an active ATPase domain should also be required for substrate degradation by RING-dead mutants. Indeed, a compound ATPase/RING domain mutant (RNF213$^{K2775A/H4014A}$) was unable to degrade CYLD or SPATA2 in the presence or absence of PTP1B (Figure 4D; Figure S5C). We also tested the effects of select MMD SNPs that affect the RING domain of RNF213,[23,48,49] by restoring doxycycline-inducible expression of *RNF213*^{C3997Y} (highly penetrant) and *RNF213*^{R4810K} (most common, low penetrance) to *RNF213*-KO BT474 and AU565 cells. As predicted, the highly penetrant, RING-mutant SNP had similar effects on SPATA2 and CYLD to RING-dead RNF213 (Figure 4E; Figure S5D).

Finally, we tested the effect of each mutant on hypoxia sensitivity in the presence or absence of *PTPN1*-KO. Consistent with the above biochemical results, cells reconstituted with tyrosine phosphorylation site-, ATPase-, RZ-, compound ATPase/RZ-, or compound RING/RZ-, mutants failed to show hypoxia hypersensitivity in response to PTP1B deficiency (Figure 4F; Figure S5E). By contrast, RING-dead RNF213 or highly penetrant MMD SNPs showed increased hypoxic cell death even in PTP1B-replete cells and almost no survival upon *PTPN1* deletion. The low penetrance, common MMD SNP RNF213^{R4810K} also showed increased cell death in hypoxia in the PTP1B-replete state, although hypersensitivity was not further enhanced by *PTPN1* deletion (Figure 4F; Figure S5E). Further studies are required to elucidate the molecular explanation for this finding; conceivably, the R4810K mutation interferes with transmission of the stimulatory effect of Y1275 phosphorylation/oligomerization to the RZ domain. In concert, though, these data indicate that tyrosine phosphorylation of RNF213 promotes ATPase-mediated oligomerization and activation of the RZ domain ubiquitin ligase activity, which in turn leads to CYLD/SPATA2 ubiquitylation, degradation, and cell death. The RING domain

inhibits the RZ domain, and MMD SNPs abrogate this regulation and promote increased CYLD/SPATA2 degradation and hypoxia hypersensitivity.

The LUBAC complex also is required for CYLD/SPATA2 degradation by RNF213

Recently, it was reported that the RZ domain ubiquitylates *Salmonella* lipopolysaccharide, most likely on its lipid component.[29] The LUBAC complex then catalyzes further ubiquitylation, promoting bacterial clearance via autophagy. Knockdown of the LUBAC complex component *RBCK1* prevented WT-RNF213-catalyzed degradation of CYLD and SPATA2 even in PTP1B-depleted BT474 or AU565 cells (Figure 5A; Figure S6A). Remarkably, however, the LUBAC complex was dispensable for CYLD/SPATA2 degradation by RING-dead RNF213. Consistent with these findings, *RBCK1* knockdown was unable to prevent hypoxia-hypersensitivity in *RNF213*-KO cells reconstituted with the RING-dead mutant (Figure 5B, Figure S6B).

RNF213, via its RZ domain, promotes NF-κB activation and primes cells for pyroptosis

CYLD and SPATA2 are important negative regulators of NF-κB, so CYLD/SPATA2 degradation would be expected to increase NF-κB activity. We used a dual luciferase reporter assay to monitor NF-κB activity in *RNF213*-KO BT474 and AU565 cells reconstituted with WT *RNF213* and various mutants with or without concomitant (pooled) *PTPN1* deletion. *RNF213*-KO cells (Vector) failed to increase reporter activity when PTP1B was depleted, while reconstituting these cells with WT-*RNF213* increased activity in *PTPN1*-KO cells to levels similar to that of parental BT474 cells with *PTPN1* deletion. RING-dead RNF213-reconstituted cells had markedly increased NF-κB activity even when *PTPN1* was intact, and activity increased further upon *PTPN1* deletion. Consistent with their effects on CYLD/SPATA2, RZ mutant, RING/RZ mutant, or ATPase/RZ mutant forms of RNF213 failed to induce NF-κB under any condition and might even have a dominant negative effect (Figure 5C; Figure S6C).

CYLD promotes apoptosis and necroptosis,[50,51] and NF-κB typically promotes cancer cell survival[52]. But PTP1B depletion or inhibition increases cell death in hypoxia, while promoting CYLD degradation and enhanced NF-κB activity. To resolve this apparent paradox, we investigated how PTP1B-deficient, hypoxic cells die, initially by testing the effects of known inhibitors of various cell death pathways. Neither ferroptosis nor necroptosis inhibitors blocked hypoxia hypersensitivity in *PTPN1*-KO cells; however, the general caspase inhibitor Z-VAD-FMK prevented hypoxia-induced cell death (Figure 5D). Similar results were obtained using SKBR3 or MDAMB361 cells (Figure S6D and S6E).

We previously observed no increase in apoptosis (a caspase-dependent process) in PTP1B-deficient breast cancer cells; instead, death appeared to be necrotic.[22] Z-VAD-FMK also inhibits "inflammatory caspases" (Caspases 1,4, and 5 in humans, Caspases 1 and 11 in mouse). Remarkably, treatment with VX765 (1 μM), a specific inhibitor of Caspase 1 and Caspase 4, completely blocked hypoxic cell death in *PTPN1*-KO BT474 cells (Figure 5E). Similar results were observed using MDAMB361 cells (Figure S6F).

NF-κB induces the expression of the inflammasome component *NLRP3*, as well as *IL1B*. The inflammasome, in turn, facilitates pro-IL-1β cleavage and release of the active cytokine, as well as the cleavage of Gasdermins.[53] Cleaved Gasdermins oligomerize and form pores in cell

membranes, leading to pyroptotic cell death. Notably, hypoxia hypersensitivity of *PTPN1*-KO BT474 or MDAMB361 cells was also blocked by treatment with the NLRP3 inhibitor MCC950 (Figure 5F; Figure S6G) or by knockout of *GSDMD* with either of two sgRNAs (Figure 5G; Figure S6H). *PTPN1*-KO also increased IL-1β production in RNF213-WT-reconsituted BT474 or AU565 cells (Figure 5H; Figure S6I). IL-1β levels increased further in cells expressing RING-dead RNF213, but there was no detectable increase in cells expressing RNF213 that cannot be tyrosine phosphorylated (Y1275F) or in RZ-dead, ATPase-dead, RING-dead and RZ-dead or RING-dead and ATPase-dead mutants.

Hypoxia-driven ER stress sends the second signal for pyroptotic cell death

NF-κB can prime cells for pyroptosis, but a "second signal" is required to trigger inflammasome assembly/inflammatory caspase activation, Gasdermin cleavage, and cell death. Several stimuli can provide the second signal, including ER stress, which is evoked by O_2 levels $\leq$1%.[54] To address the relevance of O_2 levels and its connection with ER stress, we assessed the viability of *PTPN1*-KO cells with and without CYLD or SPATA2 (Figure 6A). *PTPN1*-KO or depletion of CYLD and SPATA2 sensitized BT474 cells to death 0.1% - 0.2% O_2 (Figure 6A). At 0.5% O_2, combined *PTPN1/CYLD*-KO, *PTPN1/SPATA2*-KO, or *CYLD*-KO alone, showed increased hypoxia sensitivity. There were no significant effects of any of these mutants on viability in 1% O_2. Similar results were obtained when analogous MDAMB361-derived cell lines were studied (Figure S7A). Remarkably, *PTPN1*-KO cells treated with the IRE1α inhibitor 4μ8c were resistant to hypoxic cell death compared with DMSO control-treated cells (Figure 6B). Similar results were obtained using MDAMB361 cells (Figure S7B) or by treating *PTPN1*-KO BT474 or MDAMB361 cells with the PERK inhibitor GSK2606414 (Figure 6C; Figure S7C). These data show that ER stress signaling is required for hypoxia sensitivity in PTP1B-deficient cells.

To ask whether ER stress is sufficient to send the second signal, we treated parental BT474 cells and BT474 cells rendered SPATA2- and CYLD-deficient (by *CYLD*-KO and *SPATA2* siRNA) to mimic the effects of PTP1B deficiency in hypoxia with tunicamycin or thapsigargin in normoxia. Both agents induced cell death selectively in SPATA2- and CYLD-deficient cells (Figure 6D). Analogous results were obtained using cognate MDAMB361 cells (Figure S7D).

CYLD levels are critical for HER2+ tumor growth

To explore the potential role of CYLD in human HER2+ BC tumorigenisis, we implanted parental BT474, BT474 *PTPN1*-KO, BT474-*CYLD*-KO, and double knockout cells into the flanks of athymic *nu/nu* mice and monitored tumor development. The absence of either PTP1B or CYLD (or both) markedly inhibited tumor growth (Figure 7A). Immunoblot analysis of remant tumors from 3 mice per group confirmed the lack of PTP1B or CYLD in mice of the appropriate genotypes. Also, as predicted from our *in vitro* studies, (isolated) PTP1B deficiency resulted in lower CYLD levels (Figure 7B). Histological staining (H&E) showed increased necrosis in *PTPN1*-KO, *CYLD*-KO or *PTPN1*/*CYLD*-KO tumors compared with those from parental BT474 cells, even though the former were much smaller (Figure 7C). Moreover, there was no apparent difference in cell proliferation (Ki67) as a consequence of *PTPN1*-KO, *CYLD*-KO or *PTPN1/CYLD*-KO compared to the BT474 parental (Figure 7C).

Discussion

We have uncovered a unique mechanism of inflammatory cell death in breast cancer cells exposed to hypoxia (Figure 7D). We find that RNF213, the product of the major susceptibility gene for MMD, is phosphorylated at Y1275. Y1275 phosphorylation promotes RNF213 oligomerization, and is reciprocally regulated by ABL1,2 and PTP1B. Oligomerization activates the RNF213 RZ domain to catalyze CYLD/SPATA2 ubiquitylation and degradation. The LUBAC complex also is required for RNF213-initiated degradation of CYLD/SPATA2, but this requirement is abrogated in MMD SNPs or by engineered mutants that inactivate the RNF213 RING. Decreased CYLD/SPATA2 levels lead to increased NF-κB activation in hypoxia, which promotes *NLRP3* transcription. A second signal, most likely hypoxia-induced ER stress, promotes inflammasome assembly and activation, leading to pro-IL-1β processing/secretion and GSDMD-dependent pyroptotic cell death. Our results, combined with previous reports, provide new insights into the hypoxia response, tumor biology, RNF213 regulation, and MMD pathogenesis. The pathway revealed here, possibly in concert with other RNF213 interactors identified by our proximity ligation screen, could also contribute to common disorders such as myocardial infarction/stroke and lipotoxicity (e.g., hepatic steatosis).

Hypoxic regions in tumors typically are therapy-resistant and constitute a cellular reservoir for tumor recurrence.[3,7] PTP1B inhibition or degradation (e.g., using PROTAC technology)[55] can kill these hypoxic cells and could be useful in combination with other anti-neoplastics. Importantly, we find that PTP1B inhibition/deficiency induces pyroptosis, an inflammatory form of cell death, which could help "turn cold tumors hot" and promote the anti-tumor immune response.[53] However, inflammation also can suppress tumor immunity;[53] notably, PTP1B inhibition/deficiency increases IL-1β production, which promotes immunosuppression by myeloid cells.[56] PTP1B also has direct effects in myeloid cells[57] and lymphocytes[58,59]; whether the PTP1B/RNF213/CYLD/SPATA2 pathway is active in these cells remains unclear. A PTP1B/TCPTP inhibitor is in clinical trials as an anti-neoplastic agent[34] (NCT04777994), mainly because of its predicted immunostimulatory effects.[58,60] Our results suggest that PTP1B inhibition might also have important, salutary direct effects on tumors cell. Elucidating the cell-autonomous and non-autonomous effects of such agents, including if/how TCPTP inhibition affects RNF213, should aid in their rational deployment. It also will be important to test whether PTP1B controls hypoxia sensitivity in other tumor types, such as pancreas cancer, which is notoriously hypoxic.[61]

NF-κB signaling is activated in hypoxia through IKKβ, but the detailed mechanism has remained unclear. Scholz *et al.*[62] reported that components of the TRAF6 complex (OTUB, UVEV1a) associate with PHD1 and that multiple NF-κB pathway components are ubiquitylated. Our results indicate that hypoxia also promotes NF-κB activation via degradation of a major deubiquitylase complex. HPV-infected cells activate NF-κB in hypoxia via CYLD degradation.[63] Intriguingly, degradation requires E6, but not E6AP, the ubiquitin ligase that typically mediates E6 action. It will be interesting to test whether RNF213 is involved in this process.

Most previous studies of RNF213 have focused on its E3-ubiquitin ligase domains, although it is known that its E3 ligase activity requires ATPase function and, most likely, hexamerization.[29] Oligomerized RNF213 serves as a sensor for ISG15,[64] but to our knowledge, reciprocal control of Y1275 phosphorylation by ABL1/2 and PTP1B is the first example of a

signaling pathway regulating RNF213 oligomerization/E3 activation. We also find that the RZ domain, previously implicated in lipid ubiquitylation, has protein targets (CYLD/SPATA2). How a single E3 can have such dual activities awaits futher biochemical/structural investigation.

Our results also yield several new clues into MMD pathogenesis. RNF213-catalyzed CYLD/SPATA2 degradation provides a mechanistic explanation for earlier reports that RNF213, and to a greater extent, MMD-associated SNPs, activate NF-κB.[30] MMD is characterized by precocious carotid occlusions and stroke. Our finding that the most common RNF213 SNPs activate the RZ domain and confer LUBAC-independence on CYLD/SPATA2 degradation (and consequently, NF-κB activation and increased inflammation) could explain how these alleles promote vascular disease. MMD is also associated with Graves' disease, systemic lupus erythematosus, Sjögren's syndrome, multiple sclerosis, rheumatoid arthritis, and other immune/inflammatory disorders.[65,66] Bypassing the LUBAC complex requirement for CYLD/SPATA2 degradation/NF-κB signaling could help explain these associations.

Finally, disordered regulation of SPATA2/CYLD and possibly other RNF213 interactors could be relevant to more common diseases. Inflammation is closely associated with the early stages of stroke.[67] Stroke can trigger pyroptosis in multiple cell types in the brain including microglia, neurons, astrocytes, and brain endothelial cells.[67] Interestingly, several other RNF213 interactors (MAP4K4, SPTLC1, SARS2) are associated with atherosclerotic disorders including stroke. In concert, these results raise the possibility that inhibition of the RNF213 AAA-ATPase or RZ domains or RNF213 degraders could have therapeutic benefit in limiting brain death in stroke patients. RNF213 deficiency also abrogates lipotoxicity caused by saturated fatty acids *in vitro*[32]. It will be interesting to see if cell death in this setting is pyroptotic and mediated by the RZ domain; notably, saturated fatty acids can induce ER stress[68] and provide the "second signal" for pyroptosis.[69] If so, RNF213 modulators might have therapeutic benefit in, for example, non-alcoholic fatty acid disease. Future research will investigate whether some/all of these proteins are also RNF213 substrates and if so, whether and how they contribute to the pathogenesis of more common stenooclusive disorders.

Acknowledgements

This work was funded by RO1 CA049152, RO1 CA264933, and P30 CA016087 to B.G.N. We thank the Perlmutter Cancer Center Proteomics Research Laboratory (PRL) and Experimental Pathology Laboratory (ExPath), supported in part by P30CA016087, for technical support and help with data analysis and interpretation. Mass spectrometric experiments were also supported by NIH shared instrumentation grant 1S10OD010582-01A1. We thank Drs. Leslie Mitchell and Jef D. Boeke from the Institute of System Genetics, NYU Grossman School of Medicine for help with purification of full-length RNF213, supported by CEGS grant 1RM1HG009491.

Author Contributions

A.B. conceptualized the project, designed and performed all experiments except MS analysis, curated and analyzed the data, and wrote initial drafts of the manuscript. M.A. performed LC MS/MS experiments to identify RNF213-interacting proteins/substrates. B.U. supervised all proteomics experiments. B.G.N. conceptualized the project, provided supervision, funding, and project administration, and wrote/edited the final manuscript.

Declaration of interests

B.G.N. is the co-founder of Northern Biologics, Limited, Navire Pharma, Lighthorse Therapeutics,and Aethon Therapeutics, from which he has received consulting fees and equity. His spouse owns equity in Moderna Inc, Revolution Medicines Inc, and during the course of this work, also owned equity in Mirati Therapeutics and Amgen. He also serves on the Scientific Advisory Boards of Arvinas and Recursion Pharma and receives consulting fees and equity from the former and equity from the latter. A.B. and B.G.N. have submitted a provisional patent application related to this work.

Inclusion and diversity

We support inclusive, diverse, and equitable conduct of research.

Figure Legends

Figure 1. RNF213 phosphorylation at Y1275 is regulated by PTP1B and ABL1/2 and controls oligomerization

(A) RNF213 Y1275 phosphorylation regulates interaction with PTP1B substrate-trapping mutant. BT474 *RNF213*-KO-*PTPN1*-KD cells, with or without stable expression of a doxycycline (Dox)-inducible, HA-tagged substrate trapping mutant (D181A) of mouse PTP1B (HA-*Ptpn1*$^{D/A}$), were transiently transfected with 3x-FLAG-*RNF213* or 3x-FLAG-RNF213^{Y1275F} and exposed to 0.5 µg/ml Dox (+) or left untreated (-). Lysates (left) were subjected to anti-HA immunoprecipitation and immunoblotting for the indicated proteins (right). ERK2 serves as a loading control.

(B) Y1275 is phosphorylated in BT474 cells. BT474 *RNF213*-KO-*PTPN1*-KD cells were transiently transfected with 3x-FLAG-*RNF213* or 3x-FLAG-*RNF213*^{Y1275F}. Lysates were subjected to anti-FLAG immunoprecipitation and immunoblotting, as indicated, and pY/FLAG signal (each in arbitrary units) was quantified.

(C) Y1275 phosphorylation promotes RNF213 oligomerization. BT474 *RNF213*-KO-*PTPN1*-KD cells were transiently transfected with *GFP-RNF213* and 3x-FLAG-*RNF213* or 3x-FLAG-*RNF213*^{Y1275F}. Lysates were subjected to anti-FLAG immunoprecipitation/immunoblotting. Vinculin serves as a loading control.

(D) ABL kinases promote RNF213-mediated hypoxia hypersensitivity. BT474 and BT474 *PTPN1*-KO cells were treated with the indicated kinase inhibitors. Cells were subjected to 0.1 % O_2 for 55 hours, and viable cells were counted. Error bars represent $\pm$ S.E.M..

(E) Dasatinib inhibits RNF213-PTP1B interaction. BT474 *RNF213*-KO-*PTPN1*-KD cells expressing substrate trapping mutant HA-*Ptpn1*$^{D/A}$ were transiently transfected with 3x-FLAG-*RNF213* and then treated with dasatinib or vehicle (DMSO) for 24 hours. Cell lysates were subjected to anti-HA immunoprecipitation/immunoblotting.

(F) Dasatinib inhibits tyrosine phosphorylation of RNF213. BT474 *RNF213*-KO-*PTPN1*-KD cells were transiently transfected with 3x-FLAG-*RNF213* followed by treatment with DMSO or dasatinib for 24 hours, and lysates were subjected to anti-FLAG immunoprecipitation/immunoblotting.

(G) ABL phosphorylates RNF213 on Y1275. 3x-FLAG-RNF213 and 3x-FLAG-RNF213^{Y1275F} were purified and phosphorylated *in vitro* with the indicated amounts of recombinant ABL1 (see Methods)

(H) ABL1/ABL2 promotes RNF213 mediated hypoxia hypersensitivity in *PTPN1*-KO cells. BT474 and BT474 *PTPN1*-KO cells were transfected with *ABL1* and/or *ABL2* siRNAs targeting or control non-targeting siRNA. Cells were subjected to 0.1% O_2 for 55 hours, and viable cells were counted (top).

Error bars represent $\pm$ S.E.M. Bottom panel shows immunoblots for the indicated proteins. All experiments (A-G) are representative results from three independent experiments except for the quantifications in B, D, F, H, which are pooled data from the triplicates. Panels B, F were analyzed by ratio paired two-tailed t-test; all other results were evaluated by two-way ANOVA (analysis of variance), *P<0.05, ****P<0.0001, ns=non-specific band.

Figure 2. RNF213 interacts with CYLD/SPATA2

(A) Schematic showing proximity-based labelling of RNF213 interactors. HeLa FlpIn-TRex cells expressing TurboID (control), TurboID-RNF213 (N-Turbo) or RNF213-TurboID (C-Turbo) were used for proximity-based biotin labeling.
(B) One- sided volcano plot showing the fold-change and SAINT score of proteins identified in C-Turbo versus Control Turbo. Proteins with a SAINT Score >5% FDR are highlighted and considered to be potential interacting partners of RNF213.
(C) CYLD and SPATA2 are in proximity with RNF213. Lysates prepared as in Figure 2A were subjected to streptavidin affinity purification and immunoblotting for the indicated proteins.
(D) CYLD and SPATA2 interact with RNF213. BT474 *RNF213*-KO-*PTPN1*-KD cells were transiently transfected with 3x-FLAG-*RNF213*, and lysates were subjected to immunoprecipitation and immunoblotting as indicated.
(E and F) CYLD (E) and SPATA2 (F) protect against hypoxia hypersensitivity. BT474 and BT474 *PTPN1*-KO cells, with or without CYLD, were subjected to 0.1% O_2 for indicated times, and viable cells were counted (top). Immunoblots (bottom) show absence of CYLD/SPATA2 in stable pools generated with the indicated sgRNAs.
Error bars represent ± S.E.M. B, E, F are pooled results from three biological replicates; all other data are representative of these replicates, ****P<0.0001, two-way ANOVA.

Figure 3. Role of RNF213 RZ and RING domains in CYLD and SPATA2 ubiquitylation
(A) RNF213 promotes SPATA2 and CYLD ubiquitylation. BT474 and BT474 *RNF213*-KO cells were co-transfected with expression contructs for HA-ubiquitin (HA-UB) and ALFA-*SPATA2* or ALFA-*CYLD* and treated with claramine or vehicle (-), as indicated. Lysates (left) were subjected to anti-ALFA immunoprecipitation/immunopblotting (right).
(B) Domain map of RNF213. Critical residues for RING (H4014) and RZ (H4509) domains are indicated.
(C-F) Opposing actions of RNF213 RZ and RING domains in CYLD and SPATA2 ubiquitylation.Purified wild type or mutant 3x-FLAG-RNF213 was added to *in vitro* ubiquitylation assays with UBE2L3, CYLD, and/or SPATA2 and immunoblotted, as indicated. Each blot is representative of two biological replicates, ns=non-specific band.

Figure 4. RNF213 RING mutants/highly penetrant MMD SNPs activate RZ domain and require ATPase activity.
(A) Schematic showing key domains in RNF213. Critical residues that regulate ATPase (Y1275, K2775), RING, and RZ domains, as well as the positions of select MMD SNPs, are indicated.
(B-E) BT474 *RNF213*-KO cell reconstituted with $RNF213^{WT}$, the indicated RNF213 mutants, parental BT474 cells, and BT474 *RNF213*-KO cells with or without PTP1B, were subjected to 0.1% O_2 for 40 hours. Immunoblotting was performed for the indicated proteins.
(F) RZ and ATPase domains of RNF213 are required for hypoxia hypersensitivity of BT474 *PTPN1*-KO cells. Cells prepared as in a-d were subjected to 0.1% O_2, and viable cells were counted after 55 hours.
Error bars represent ± S.E.M. (n = 3 biological replicates, each panel) and each blot is representative of two biological replicates. ****P<0.0001, two-way ANOVA, ns=non-specific band.

Figure 5. *PTPN1*-KO cells die via RNF213- and LUBAC-dependent pyroptosis
(A) Wild-type, but not RING-dead RNF213 requires LUBAC for CYLD/SPATA2 degradation. BT474 *RNF213*-KO cells reconstituted with wild-type *RNF213* or *RNF213*^{H4014A} parental BT474 cells and BT474 *RNF213*-KO with or without PTP1B were transfected with *RBCK1* or control siRNA. Cells were subjected to 0.1% O_2 for 40 hours, lysed, and, immunoblotted as indicated (top). *RBCK1* knockdown was confirmed by RT-qPCR (bottom).
(B) RING-dead RNF213 bypasses LUBAC requirement. The indicated cells were subjected to 0.1% O_2 for 55 hours, and viable cell numbers were counted.
(C) RNF213 promotes NF-κB activity. Cells described in Figure 4F were transfected with an NF-κB reporter construct (see Methods) and subjected to 0.1% O_2 for 48 hours. Firefly and Renilla luciferase signals were measured, reporter activity was quantified as the ratio of Firefly/Renilla signal, and all other signals were normalized to that from parental BT474 cells.
(D) Hypoxic cell death in *PTPN1*-KO cells is caspase-dependent. BT474 and BT474 *PTPN1*-KO cells were treated with the indicated inhibitors, placed in 0.1% O_2 for 55 hours, and cell viability was assessed.
(E and F) Hypoxic cell death in *PTPN1*-KO cells requires inflammatory caspases and the inflammasome. As in D, except with/without VX765 (E) or MCC950 (F).
(G) GSDMD promotes hypoxic cell death of *PTPN1*-KO cells. Pools of BT474 and BT474 *PTPN1*-KO cells, with or without *GSDMD* deletion, were subjected to 0.1% O_2, and cell viability was measured at 55 hours (top). Immunoblot indicates efficiency of *GSDMD* knockout (bottom).
(H) Hypoxia-hypersensitive cells release IL-1β. Cells prepeared as in Figure 4E were subjected to 0.1% O_2 for 55 hours, and IL-1β in supernatants was quantified by immunoassay.
In all panels, error bars represent ± S.E.M. (n = 3 biological replicates) and each blot is representative of two biological replicates.****P<0.0001, two-way ANOVA, ns=non-specific band.

Figure 6. Hypoxia-evoked ER stress activates the inflammasome for RNF213-triggered pyroptosis.
(A) Hypoxia hypersensitivity is dependent on O_2 levels. BT474 and BT474 *PTPN1*-KO cells were subjected to varying levels of O_2 (0.1, 0.2, 0.5 and 1% O_2) for 55 hours, and viability was assessed.
(B and C) ER stress promotes hypoxia hypersensitivity. BT474 and BT474 *PTPN1*-KO cells treated with the IRE1α inhibitor 4μ8C (B) or the PERK inhibitor GSK2606414 (C), were subjected to 0.1% O_2 for 55 hours, and viability was assessed.
(D) ER stress causes pyroptosis in CYLD/SPATA2-deficient cells in normoxia. BT474 cells, with or without CYLD/SPATA2, were treated with tunicamycin (10 μM) or thapsigargin (5 μM) for 40 hours, and cell viability was measured at 40 hours. Error bars represent ± S.E.M (n = 3 biological replicates), ****P<0.0001, two-way ANOVA.

Figure 7. The PTP1B/RNF213/CYLD/SPATA2 pathway controls HER2+ breast cancer tumorigenesis
(A-C) CYLD is critical for HER2+ breast tumorigenesis. BT474 and BT474 *PTPN1*-KO cells, with or without *CYLD*-KO, were injected subcutaneously into athymic *nu/nu* mice (6/group). Tumor size was measured weekly for 9 weeks (A). Residual tumors were excised, and analyzed by

immunoblotting (B) and histology/immunohistochemistry (C). * in (C) indicates representative necrotic regions. Error bars represent ± S.E.M., ***P<0.001, two-way ANOVA.
(D) Left panel: ABL1/2-catalyzed phosphorylation of RNF213 at Y1275 promotes RNF213 oligomerization; PTP1B dephosphorylates this site. Oligomerized RNF213, via its RZ domain, ubiquitylates CYLD and SPATA2, and further ubiquitylation, catalyzed by the LUBAC complex, promotes CYLD/SPATA2 degradation.
Left middle panel: ATPase-dead RNF213 cannot oligomerize and does not promote hypoxia hypersensitivity.
Right middle panel:RING-dead RNF213 enhances RZ-mediated ubiquitylation of CYLD/SPATA2 and leads to CYLD and SPATA2 degradation even in the absence of LUBAC. Degradation of CYLD/ SPATA2 leads to increased NF-κB signaling, priming pyroptosis. Hypoxia-associated ER-stress provides the "second signal" to activate the inflammasome formation, leading to RNF213-driven pyroptotic cell death.
Right panel: RZ-dead or RING/RZ-dead RNF213 cannot ubiquitylate CYLD/SPATA2 and does not promote hypoxia hypersensitivity in response to PTP1B inhibition.

SUPPLEMENTAL INFORMATION

Figure S1. Y1275 phosphorylation is regulated by PTP1B and controls RNF213 oligomerization.
(A) PTP1B inhibitor sensitizes multiple breast cancer subtypes to hypoxia. The indicated cell lines were treated with the PTP1B inhibitor claramine, placed in 0.1% O_2 for 55 hours, and viable cells were counted.
(B) Spectrum supporting phosphorylation of RNF213-Y1275 on peptide EAAEPLSEPKEDQEAAELLSEPEEESERHILELEEVYDYLYQPSYR, from 3x-FLAG-RNF213-TurboID-enriched samples. The HCD MS/MS spectra of sextuply charged m/z 922.9244 ion recorded in the ion trap of an Orbitrap Eclipse is shown. Observed N-terminal sequence ions (b-ions) are shown in blue, and C-terminal fragment ions (y-ions) are shown in red. Backbone cleavages are indicated in the peptide sequence, and the phosphorylated tyrosine is indicated (red).
(C) Y1275 phosphorylation affects RNF213-PTP1B interaction. AU565 *RNF213*-KO-*PTPN1*-KD cells with or without stable expression of doxycycline (Dox)-inducible, HA-*Ptpn1*$^{D/A}$ were transiently transfected with 3x-FLAG-*RNF213* or 3x-FLAG-RNF213^{Y1275F} and exposed to 0.5 µg/ml Dox (+) or left untreated (-). Lysates (top) were subjected to anti-HA immunoprecipitation and immunoblotting for the indicated proteins (bottom). ERK2 serves as a loading control.
(D) RNF213-Y1275 is also phosphorylated in AU565 cells. AU565 *RNF213*-KO-*PTPN1*-KD cells were transiently transfected with 3x-FLAG-*RNF213* or 3x-FLAG-*RNF213*^{Y1275F}. Lysates were subjected to anti-FLAG immunoprecipitation and immunoblotting, as indicated, and pY/FLAG signal (each in arbitrary units) was quantified.
(E) Y1275 phosphorylation promotes RNF213 oligomerization. AU565 *RNF213*-KO-*PTPN1*-KD cells were transiently transfected with expression vectors for *GFP-RNF213* and 3x-FLAG-*RNF213* or 3x-FLAG-*RNF213*^{Y1275F}. Lysates were subjected to anti-FLAG immunoprecipitation/immunoblotting. Vinculin serves as a loading control.
Error bars represent $\pm$ S.E.M.. A, D (lower) are pooled results from three biological replicates; all other data except (B) are representative of these replicates. A, E were evaluated by two-way ANOVA, whereas D was analyzed by ratio paired two-tailed t-test, $^{**}P<0.01$, $^{***}P<0.001$, $^{****}P<0.0001$, ns=non-specific band.

Figure S2. ABL phosphorylates RNF213 on Y1275.
(A) SKBR3 and SKBR3 *PTPN1*-KO cells were treated with the indicated inhibitors. Cells were subjected to 0.1% O_2 for 36 hours, and viable cells were counted.
(B) Dasatinib inhibits RNF213-PTP1B interaction. AU565 *RNF213*-KO-*PTPN1*-KD cells expressing substrate trapping mutant HA-*Ptpn1*$^{D/A}$ were transiently transfected with expression vector for 3x-FLAG-*RNF213*, then treated with dasatinib or vehicle (DMSO) for 24 hours. Lysates were subjected to anti-HA immunoprecipitation/ immunoblotting.
(C) Dasatinib inhibits tyrosine phosphorylation of RNF213. AU565 *RNF213*-KO-*PTPN1*-KD cells were transiently transfected with 3x-FLAG-*RNF213* followed by treatment with DMSO or dasatinib for 24 hours. Lysates were subjected to anti-FLAG immunoprecipitation/ immunoblotting.
(D) Purity of 3x-FLAG-RNF213 and 3x-FLAG-RNF21^{Y1275F} proteins (see Methods)

(E) ABL phosphorylates RNF213 on Y1275. Purified 3x-FLAG-RNF213 and 3x-FLAG-RNF213^{Y1275F} were phosphorylated *in vitro* with recombinant His-ABL1 for the indicated times (see Methods)
(F) ABL1/ABL2 promote RNF213-mediated hypoxia hypersensitivity in *PTPN1*-KO cells. MDAMB361 and MDAMB361 *PTPN1*-KO cells were transfected with siRNAs targeting *ABL1* and/or *ABL2* or control non- targeting siRNA. Cells were subjected to 0.1% O_2 for 48 hours, and viable cells were counted (top). Immunoblot shows knockdown efficiency (bottom).
Error bars represent ± S.E.M. All panels (A-F) are representative results from two independent experiments, except for the quantifications in A, C, F, which are pooled data from triplicates. A, F were evaluated by two-way ANOVA; C was analyzed by ratio paired two-tailed t-test
***P*<0.01, *****P*<0.0001, ns=non-specific band.

Figure S3. Sample preparation for proximity-based labelling screen.
(A) HeLa FlpIn-TRex cells reconstituted with Control Turbo, N-turbo, or C-turbo were induced with 0.5 μg/ml of Dox. Post-biotin labelling (see Methods), lysates (left) were subjected to streptavidin affinity purification (right) and immunoblotting.
(B) Silver-stained SDS-PAGE gel showing that comparable amounts of streptavidin-purified proteins were submitted for mass spectrometry.
(C) One-sided volcano plot showing fold-change and SAINT score of proteins identified in N-Turbo versus Control Turbo. Proteins with SAINT Score >5% FDR are highlighted.
(D and E) GO pathway analysis showing top 10 enriched molecular functions of C-Turbo (D)- and N-Turbo (F)-interacting proteins.

Figure S4. CYLD/SPATA2 are relevant substrates of RNF213 in mediating hypoxia hypersensitivity.
(A and B) SKBR3 and SKBR3 *PTPN1*-KO cells, with or without CYLD (A) or SPATA2 (B) , were subjected to 0.1% O_2 for the indicated times, and viable cells were counted (top). Immunoblots (bottom) show absence of CYLD/SPATA2 in stable pools generated with the indicated sgRNAs.
(C) RNF213 promotes SPATA2 and CYLD ubiquitylation. AU565 and AU565 *RNF213*-KO cells were co-transfected with expression contructs for HA-UB and ALFA-*SPATA2* or ALFA-*CYLD* and treated with claramine or vehicle (-), as indicated. Lysates (left) were subjected to anti-ALFA immunoprecipitation/immunoblotting (right).
(D) Purity of 3x-FLAG-RNF213, 3x-FLAG-RNF21^{H4509A}, 3x-FLAG-RNF21^{H4014A}, 3x-FLAG-RNF21$^{H4014A/H4509A}$ after indicated steps (see Methods)
(E and F) Effects of RNF213 mutants on global ubiquitylation. Hela FlpIn-TRex *RNF213*-KO (E) and BT474 *RNF213*-KO (F) cells were co-transfected with expression contructs for HA-UB and 3x-FLAG-tagged *RNF213* or -*RNF213*^{H4014A} --*RNF213*^{H4509A} or -*RNF213*$^{H4014A/H4509A}$. Cells were subjected to 0.1% O_2 for the indicated times, and lysates were subjected to immunoblotting.
Error bars represent ± S.E.M.. A and B are pooled results from three biological replicates; data in C, E and F are representative of replicates, *****P*<0.0001, two-way ANOVA, ns=non-specific band.

Figure S5. RNF213 RING mutants/highly penetrant MMD SNPs activate RZ domain and require ATPase activity.

(A-D) AU565 *RNF213*-KO cell reconstituted with RNF213^{WT} or the indicated RNF213 mutants, parental AU565 cells, and AU565 *RNF213*-KO cells with or without *PTPN1* deletion, were subjected to 0.1% O_2 for 40 hours. Immunoblotting was performed for the indicated proteins.
(E) RZ and ATPase domains of RNF213 are required for hypoxia hypersensitivity of AU565 *PTPN1*-KO cells. Cells prepared as in A-D were subjected to 0.1% O_2, and viable cells were counted after 48 hours.
Error bars represent ± S.E.M.. (n = 3 biological replicates, each panel); each blot is representative of two biological replicates. ***P<0.001, ****P<0.0001, two-way ANOVA, ns=non-specific band.

Figure S6. *PTPN1*-KO cells die via RNF213- and LUBAC-dependent pyroptosis.
(A) Wild-type, but not RING-dead, RNF213 requires LUBAC for CYLD/SPATA2 degradation. AU565 *RNF213*-KO cells reconstituted with wild-type *RNF213* or *RNF213*^{H4014A}, parental AU565 cells. and AU565 *RNF213*-KO cells with or without *PTPN1* deletion were transfected with *RBCK1* or control siRNAs. Cells were subjected to 0.1% O_2 for 40 hours, lysed, and immunoblotted as indicated (top). *RBCK1* knockdown was confirmed by RT-qPCR (bottom).
(B) RING-dead RNF213 bypasses LUBAC requirement. The indicated cells were subjected to 0.1 % O_2 for 48 hours, and viable cell numbers were counted.
(C) RNF213 promotes NF-κB activity. The cells described in Figure S5E were transfected with an NF-κB reporter construct (see Methods) and subjected to 0.1% O_2 for 40 hours. Firefly and Renilla luciferase signals were measured, reporter activity was quantified as the ratio of Firefly/Renilla signal, and all signals were normalized that from parental AU565 cells.
(D and E) Hypoxic cell death in *PTPN1*-KO cells is caspase-dependent. SKBR3 and SKBR3 *PTPN1*-KO (D) and MDAMB361 and MDAMB361 *PTPN1*-KO (E) cells were treated with the indicated inhibitors, placed in 0.1% O_2 for 40 (D) or 48 (E) hours, and cell viability was assessed.
(F and G) Hypoxic cell death in MDAMB361 *PTPN1*-KO cells requires inflammatory caspases and the inflammasome. As in (E), except with/without VX765 (F) or MCC950 (G).
(H) GSDMD promotes hypoxic cell death of *PTPN1*-KO cells. Pools of MDAMB361 and MDAMB361 *PTPN1*-KO cells, with or without *GSDMD* deletion, were subjected to 0.1% O_2, and cell viability was measured at 48 hours (top). Immunoblot indicates efficiency of *GSDMD* knockout (bottom).
(I) Hypoxia-hypersensitive cells release IL-1β. Cells prepared as in Figure S5E were subjected to 0.1% O_2 for 48 hours, and IL-1β in supernatants was analyzed by immunoassay.
In all panels, error bars represent ± S.E.M. (n = 3 biological replicates), and each blot is representative of two biological replicates. ***P<0.001, ****P<0.0001, two-way ANOVA, ns=non-specific band.

Figure S7. Hypoxia-evoked ER stress activates the inflammasome for RNF213-triggered pyroptosis.
(A) Hypoxia hypersensitivity is dependent on O_2 level. MDAMB361 and MDAMB361 *PTPN1*-KO cells were subjected to varying levels of O_2 (0.1, 0.2, 0.5 and 1% O_2) for 55 hours, and viability was assessed.

(B and C) ER stress promotes hypoxia hypersensitivity. MDAMB361 and MDAMB361 *PTPN1*-KO cells treated with the IRE1α inhibitor 4μ8C (B) or the PERK inhibitor GSK2606414 (C), were subjected to 0.1 % O_2 for 48 hours, and viability was assessed.
(D) ER stress causes pyroptosis in CYLD/SPATA2-deficient cells in normoxia. MDAMB361 cells, with or without CYLD/SPATA2, were treated with tunicamycin (10 μM) or thapsigargin (5 μM) for 40 hours and viability was assessed. Error bars represent ± S.E.M.. (n = 3 biological replicates), ****P<0.0001, two-way ANOVA.

STAR METHODS

Cell culture and cell line generation

Sources of the breast cancer cell lines used here were described;[70] all are maintained as frozen stocks by the Neel Laboratory. Except where indicated, cells were cultured in DMEM +10% FBS with 100 U/ml penicillin and 100 mg/ml streptomycin at 37°C in 5% CO_2 and tested monthly for mycoplasma by PCR.

Isogenic HeLa Flp-In T-Rex *RNF213*-KO cells that inducibly express wild-type *RNF213* or *RNF213* variants in response to doxycycline (DOX) were generated by co-transfecting pcDNA5/FRT/TO-based expression constructs with 3x-Flag tagged *RNF213* or *RNF213* variant with pOG44, which directs constitutive expression of Flp recombinase (FLP). Cells with successful integration were selected by adding hygromycin B (200 µg/ml) 48 hours post-transfection. Single cell clones of *RNF213*-deleted HeLa, BT474, and AU565 cells, or of *PTPN1*-deleted BT474, SKBR3, and MDAMB361 cells, were generated by using CRISPR/Cas9 technology.[71] Briefly, sgRNAs targeting each gene were cloned into the BbsI site of pSpCas9 (BB)–2A–Puro (PX459; Addgene), and cells were transfected with each cloned vector using Lipofectamine™ 3000 Transfection Reagent (ThermoFisher Scientific). After 48 hours, cells were diluted into 96-well plates (1 cell/well) containing 48-hour conditioned media from the same line in addition to standard media. Knockout clones were confirmed by immunoblotting. The sgRNA sequences are shown in key resources table.

Piggbac (PB)-based expression was used to re-express WT *RNF213* or RNF213 variants under Dox control in *RNF213*-KO BT474 and *RNF213*-KO AU565 cells. Briefly, PB-TA-ERN (Addgene)-based expression constructs containing RNF213 and RNF213 variants were co-transfected with transposase expression vector, and integrants were selected by adding G418 (800µg/ml). RNF213 expression was induced by adding 0.5 µg/ml Dox.

PTPN1 depletion was accomplished by stable shRNA knockdown using pSUPER-Puro-based retroviral vectors. *RBCK1*, *ABL1*, and *ABL2* ON-TARGETplus siRNA (Horizon Discovery) were introduced using Lipofectamine™ RNAiMAX reagent (ThermoFisher Scientific). Pooled knockout lines were generated by infection with lentiviruses expressing CAS9 and appropriate sgRNAs. Lentiviruses and retroviruses were packaged as described.[72]

Viability assays

Cells were seeded in 6-well plates (2 X 10^6/well for MDAMB361, 1.5 X 10^6/well for other lines) and maintained in at 37°C, 5% CO_2. After 24 hours, viable cell number was determined by Trypan Blue exclusion , and fresh media was added to replicates placed in a standard incubator (normoxia) and in hypoxic conditions (0.1% O_2, Whitley H35 Hypoxystation). Viable cells were counted at various times, as indicated.

Generation of *RNF213* mutants

RNF213 mutants were generated by PCR or by using fragments synthesized by Genewiz/IDT. Fragments containing the desired mutation were sequenced, digested, and cloned into wild-type RNF213 plasmids by using T4 DNA ligase or via Gibson assembly[73].

NF-κB reporter assays

Cells co-transfected with an NF-κB reporter construct (p2X-NF-κB-BS-Luc-Firefly, a generous gift of Dan Littman, NYU Grossman School of Medicine) and pCMV-Renilla, were subjected to 0.1 % O_2 for the indicated times. Firefly and Renilla luciferase was measured using the Dual-Luciferase® Reporter Assay System (Promega) according to the manufacturer's instructions. Reporter activity was quantified as the ratio of Firefly/Renilla signal, and all signals were normalized to the signal in parental BT474 cells.

IL-1β assays

Cell supernatants were collected at the indicated times, and IL-1β levels were quantified by using the Lumit™ IL-1β Immunoassay (Promega), according to manufacterer's instructions.

Biochemical Assays

Immunoblotting and immunoprecipitations

Cells were lysed in RIPA (total cell lysates, ALFA-tag precipitations) or NP40 buffer (co-immunoprecipitations); buffer compositions and immunoprecipitation conditions have been described[27] (also see **Method details**). ALFA-tagged proteins were recovered using a single domain camelid antibody bound to magenetic beads (NanoTag Biotechnologies). Antibody details are in key resources table.

Proximity-based labelling

Cells were cultured in standard media but with 10% tetracycline (Tet)-free FBS (Clonetech) for at least 1 week. Tet-free/biotin-free FBS was generated by incubating Tet-free FBS with sterile streptavidin beads overnight followed by centrifugation to remove the beads. N-Turbo, C-Turbo, and Turbo proteins were induced by adding 1 µg/ml Dox to cells for 36 hours. For the last ten min. of incubation, 500 µM of biotin was added to the medium. Labelling reactions was terminated by removing the medium and adding ice-cold PBS to plates, which were kept on ice. Lysates were collected in RIPA buffer without Na-deoxycholate, and biotin-labelled proteins were collected by incubating with high capacity streptavidin agarose beads for 4 hours at 4°C. Comparable protein amounts (assessed by silver stain and avidin blotting) were analyzed by MS.

Purification of RNF213 and RNF213 variants

HeLa *RNF213*-KO cells expressing RNF213 or RNF213 variants (except RNF213^{H4509A}) were induced with 0.5 µg/ml Dox for 4 days. The 3x-FLAG-RNF213^{H4509A} variant was transiently transfected into HeLa *RNF213*-KO cells, as the stable expression of this variant was low. Lysates from ten 15 cm plates were subjected to anti-FLAG immunoprecipitation. RNF213 species were eluted with 3x-FLAG peptide and concentrated by passage through an Amicon Ultra-4 Centrifugal Filter (100 kDa cut-off).

***In vitro* ubiquitylation assays**

Ubiquitylation assays were performed as described.[27] Briefly, 0.25µM of purified RNF213 or RNF213 variant were incubated with 2.5µM GST-SPATA2 (Abnova) or 2.5µM 6xHis-CYLD (R&D) in E3-Ligase buffer (R&D) along with 50µM HA-Ub, 100nM UBE1 (E1), 1µM UBE2L3 (E2), and 10mM Mg-ATP (all from Boston Biochem) for 30 min. in a total reaction volume of 25

µl. Reactions were terminated by adding SDS–PAGE sample buffer followed by incubation for 5 min. at 95°C.

In vitro kinase assays

Purified full-length 3x-FLAG-tagged RNF213 or RNF213^{Y1275F} were mixed with varying amounts of bacterially produced His-ABL1 (as indicated) and incubated with 600ng of RNF213 in kinase assay buffer (50mM HEPES [pH 7.5], 10mM $MgCl_2$, 2.5mM DTT, 75µM ATP) for varying times, as indicated. Final reaction volumes were 20µl. Reactions were terminated by adding SDS–PAGE sample buffer followed by incubation for 5 min. at 95°C.

Mass spectrometry

Proteins collected on streptavidin beads were digested with sequencing grade trypsin and analyzed by LC/MS/MS using a Thermo Scientific EASY-nLC 1200 and a Thermo Scientific Orbitrap Eclipse Mass Spectrometer MS/MS spectra were searched against the Uniprot human database with the addition of the sequences of RNF213 with TurboID at the N- and C-terminus using Sequest within Proteome Discoverer 1.4. MS/MS spectra were also searched using Byonic by Protein Metrics specifically to identify phosphorylation sites on RNF213. See **Method details** for details.

Xenografts and histology

All animal experiments were approved by, and conducted in accordance, with the procedures of the Institutional Animal Care and Use Committee (IACUC) at NYU School Of Medicine (Protocol no. 170602). Six week-old female Balb/c athymic nude mice were implanted with a 60-day release pellet containing 0.72mg 17β-Estradiol (Innovative Research of America). One week later, BT474 cells or BT474 derivatives (1 x 10^6) resuspended with 50µl of Matrigel (BD), were injected subcutaneously into the right flanks of these mice. Length and width of tumors were measured weekly using Vernier calipers. Tumor volume was calculated as length x width^2 x 0.52.

For histology and immunohistochemistry, tumors were fixed in 4% paraformaldehyde (PFA) and embedded in paraffin. Sectioning and staining were performed by Perlmutter Cancer Center Experimental Pathology Core.

Quantification and statistical analysis

Graphs were generated and statistical analyses were performed using GraphPad Prism9. Multiple groups were compared by two-way ANOVA, with additional Tukey multiple comparisons test. Two group comparisons were evaluated by two-tailed t test. Values represent the mean of experiments, with error bars representing S.E.M..

METHODS DETAILS

Immunoblotting, immunoprecipitation, and SDS-PAGE

For co-immunoprecipitations, cells were lysed in NP40 buffer (50mM Tris·HCl [pH 8], 150mM NaCl, 2mM EDTA, 10mM Na4P2O7, 100mM NaF, 2mM Na3VO4, 1% [vol/vol] NP-40, 40

µg/ml phenylmethyl sulfonyl fluoride, 2 µg/ml antipain, 2µg/ml pepstatin A, 20µg/ml leupeptin, and 20µg/ml aprotinin). For streptavidin affinity purifications and standard immunoprecipitations, modified RIPA buffer (50mM Tris·HCl [pH 8], 150mM NaCl, 2mMEDTA, 10mM Na4P2O7, 100mM NaF, 2mM Na3VO4, 1% [vol/vol] NP-40, 0.1% (wt/vol) SDS, 40µg/ml phenylmethyl sulfonyl fluoride, 2µg/ml antipain, 2µg/ml pepstatin A, 20µg/ml leupeptin, and 20µg/ml aprotinin) was used for cell lysis. For detection of ubiquitylated species *in vivo*, 10mM N-ethylmaleimide (NEM) and 10mM iodoacetamide (IAM) were added to the lysis buffer.

For immunoblotting of whole cell lysates, equal amounts of protein per sample were subjected to SDS–PAGE and transferred to polyvinylidene fluoride (PVDF) membranes (Millipore). For immunoprecipitation of FLAG-tagged proteins, lysates were incubated with anti-FLAG-magnetic beads for 4 hours on a rotator-mixer at 4°C. For immunoprecipitation of HA-tagged proteins, lysates were incubated with anti-HA-agarose beads for 4 hours on a rotator-mixer at 4°C. For immunoprecipitation of ALFA-tagged proteins, lysates were incubated with ALFA-selector ST agarose beads overnight on a rotor-mixer at 4°C. For recovery of biotinylated proteins, high-capacity streptavidin agarose resin (ThermoScientific) was added to lysates, which were rotated for 4 hours at 4°C. Beads were washed five times in lysis buffer, incubated in sample buffer at 95C for 5 min. and resolved by SDS-PAGE and immunoblotting. For in vitro ubiquitylation and phosphorylation using purified RNF213 and RNF213 variants, proteins were eluted from beads by incubation with an excess of 3X-FLAG peptide. Lysates and immunoprecipitates were resolved by modified SDS–PAGE on 3–8% Tris-acetate gels (Novex) or 5% Tris-glycine gels. Gels were transferred in 1× transfer buffer, 10% methanol for 1 hour at 25 V using an XCell II Blot Module (Novex) and analyzed by acquisition software (Image Studio Lite), on an Odyssey Infrared imaging system (Li-Cor Biosciences). All antibodies used are listed in key resources table.

Mass Spectrometry

Proteins bound to streptavidin agarose beads were washed with 100mM NH_4HCO_3 (pH 8), reduced with 2.5uL of 0.2M dithiothreitol at 57C for 1 hour, alkylated with 2.5uL of 0.5M IAM for 45 min. at room temperature in the dark, and digested overnight at room temperature with 500ng sequencing grade modified trypsin (Promega). After digestion, samples were acidified to a final concentration of 0.5% trifluoroacetic acid (TFA). A C18 cleanup was performed on all samples using Ultra-Micro SpinColumns (Harvard Apparatus). Briefly, samples were loaded onto equilibrated spin columns, rinsed with 0.1% TFA, and eluted with 40% acetonitrile/0.5% acetic acid and 80% acetonitrile/0.5% acetic acid. Organic solvent was removed using a SpeedVac concentrator, and all samples were reconstituted in 0.5% acetic acid.

One-third of each sample was analyzed individually by LC/MS/MS. Samples were separated online using a Thermo Scientific EASY-nLC 1200, where solvent A was 2% acetonitrile/0.5% acetic acid, and solvent B was 80% acetonitrile/0.5% acetic acid. A 60-min. gradient from 5-35%B was applied to all samples. Peptides were gradient-eluted directly to a Thermo Scientific Orbitrap Eclipse Mass Spectrometer. High resolution, full MS spectra were acquired with a resolution of 240,000, an AGC target of 1e6, a maximum ion time of 50 ms, and a scan range of 400 to 1500 m/z. Following each full MS scan, data-dependent HCD MS/MS spectra collected with low resolution at top speed with a 3ms cycle time. All MS/MS spectra

were collected with a rapid scan in the ion trap, an AGC target of 2e4, a maximum ion time of 18 ms, one microscan, 0.7 m/z isolation window, auto scan range mode, and NCE of 27. MS/MS spectra were searched against the Uniprot human database using Sequest within Proteome Discoverer. 1.4. MS/MS spectra were also searched with Byonic by Protein Metrics against a database containing just RNF213 and common contaminants to identify phosphorylation sites.

For TurboID analyses, beads were washed two times with 100mM NH_4HCO (pH 8). Samples were reduced with 2uL of 0.2M dithiothreitol at 57C for 1 hour and alkylated with 2uL of 0.5M IAM for 45 min. at room temperature in the dark. Samples were digested overnight at room temperature with 250ng sequencing trypsin. After digestion, samples were acidified to a final concentration of 0.5% trifluoroacetic acid (TFA), and cleaned up on C18 columns as above. One-third of each sample was analyzed individually by LC/MS/MS. LC conditions were identical to those above. High resolution full MS spectra were acquired with a resolution of 70,000, an AGC target of 1e6, a maximum ion time of 120 ms, and scan range of 400 to 1500 m/z. Following each full MS were 20 data-dependent high resolution HCD MS/MS spectra. All MS/MS spectra were collected with resolution of 17,500, an AGC target of 5e4, a maximum ion time of 120 ms, one microscan, 2 m/z isolation window, fixed first mass of 150 m/z, and NCE of 27. MS/MS spectra were searched against the Uniprot human database with the added sequences of RNF213 with the TurboID on the N- and C-terminus using Sequest within Proteome Discoverer 1.4.

REFERENCES

1. Bertout, J.A., Patel, S.A., and Simon, M.C. (2008). The impact of O2 availability on human cancer. Nat Rev Cancer *8*, 967-975. 10.1038/nrc2540.
2. Schofield, C.J., and Ratcliffe, P.J. (2004). Oxygen sensing by HIF hydroxylases. Nat Rev Mol Cell Biol *5*, 343-354. 10.1038/nrm1366.
3. Singleton, D.C., Macann, A., and Wilson, W.R. (2021). Therapeutic targeting of the hypoxic tumour microenvironment. Nat Rev Clin Oncol *18*, 751-772. 10.1038/s41571-021-00539-4.
4. Wouters, B.G., and Koritzinsky, M. (2008). Hypoxia signalling through mTOR and the unfolded protein response in cancer. Nat Rev Cancer *8*, 851-864. 10.1038/nrc2501.
5. Cummins, E.P., Berra, E., Comerford, K.M., Ginouves, A., Fitzgerald, K.T., Seeballuck, F., Godson, C., Nielsen, J.E., Moynagh, P., Pouyssegur, J., and Taylor, C.T. (2006). Prolyl hydroxylase-1 negatively regulates IkappaB kinase-beta, giving insight into hypoxia-induced NFkappaB activity. Proc Natl Acad Sci U S A *103*, 18154-18159. 10.1073/pnas.0602235103.
6. Rius, J., Guma, M., Schachtrup, C., Akassoglou, K., Zinkernagel, A.S., Nizet, V., Johnson, R.S., Haddad, G.G., and Karin, M. (2008). NF-kappaB links innate immunity to the hypoxic response through transcriptional regulation of HIF-1alpha. Nature *453*, 807-811. 10.1038/nature06905.
7. Eltzschig, H.K., Bratton, D.L., and Colgan, S.P. (2014). Targeting hypoxia signalling for the treatment of ischaemic and inflammatory diseases. Nat Rev Drug Discov *13*, 852-869. 10.1038/nrd4422.
8. Nizet, V., and Johnson, R.S. (2009). Interdependence of hypoxic and innate immune responses. Nat Rev Immunol *9*, 609-617. 10.1038/nri2607.
9. Pakos-Zebrucka, K., Koryga, I., Mnich, K., Ljujic, M., Samali, A., and Gorman, A.M. (2016). The integrated stress response. EMBO Rep *17*, 1374-1395. 10.15252/embr.201642195.
10. Kroemer, G., Galluzzi, L., Kepp, O., and Zitvogel, L. (2013). Immunogenic cell death in cancer therapy. Annu Rev Immunol *31*, 51-72. 10.1146/annurev-immunol-032712-100008.
11. Eltzschig, H.K., and Carmeliet, P. (2011). Hypoxia and inflammation. N Engl J Med *364*, 656-665. 10.1056/NEJMra0910283.
12. Frangioni, J.V., Beahm, P.H., Shifrin, V., Jost, C.A., and Neel, B.G. (1992). The nontransmembrane tyrosine phosphatase PTP-1B localizes to the endoplasmic reticulum via its 35 amino acid C-terminal sequence. Cell *68*, 545-560. 10.1016/0092-8674(92)90190-n.
13. Haj, F.G., Verveer, P.J., Squire, A., Neel, B.G., and Bastiaens, P.I. (2002). Imaging sites of receptor dephosphorylation by PTP1B on the surface of the endoplasmic reticulum. Science *295*, 1708-1711. 10.1126/science.1067566.
14. Elchebly, M., Payette, P., Michaliszyn, E., Cromlish, W., Collins, S., Loy, A.L., Normandin, D., Cheng, A., Himms-Hagen, J., Chan, C.C., et al. (1999). Increased insulin sensitivity and obesity resistance in mice lacking the protein tyrosine phosphatase-1B gene. Science *283*, 1544-1548. 10.1126/science.283.5407.1544.

15. Klaman, L.D., Boss, O., Peroni, O.D., Kim, J.K., Martino, J.L., Zabolotny, J.M., Moghal, N., Lubkin, M., Kim, Y.B., Sharpe, A.H., et al. (2000). Increased energy expenditure, decreased adiposity, and tissue-specific insulin sensitivity in protein-tyrosine phosphatase 1B-deficient mice. Mol Cell Biol *20*, 5479-5489. 10.1128/MCB.20.15.5479-5489.2000.
16. Zabolotny, J.M., Bence-Hanulec, K.K., Stricker-Krongrad, A., Haj, F., Wang, Y., Minokoshi, Y., Kim, Y.B., Elmquist, J.K., Tartaglia, L.A., Kahn, B.B., and Neel, B.G. (2002). PTP1B regulates leptin signal transduction in vivo. Dev Cell *2*, 489-495. 10.1016/s1534-5807(02)00148-x.
17. Cheng, A., Uetani, N., Simoncic, P.D., Chaubey, V.P., Lee-Loy, A., McGlade, C.J., Kennedy, B.P., and Tremblay, M.L. (2002). Attenuation of leptin action and regulation of obesity by protein tyrosine phosphatase 1B. Dev Cell *2*, 497-503. 10.1016/s1534-5807(02)00149-1.
18. Bentires-Alj, M., and Neel, B.G. (2007). Protein-tyrosine phosphatase 1B is required for HER2/Neu-induced breast cancer. Cancer Res *67*, 2420-2424. 10.1158/0008-5472.CAN-06-4610.
19. Julien, S.G., Dube, N., Read, M., Penney, J., Paquet, M., Han, Y., Kennedy, B.P., Muller, W.J., and Tremblay, M.L. (2007). Protein tyrosine phosphatase 1B deficiency or inhibition delays ErbB2-induced mammary tumorigenesis and protects from lung metastasis. Nat Genet *39*, 338-346. 10.1038/ng1963.
20. Cancer Genome Atlas, N. (2012). Comprehensive molecular portraits of human breast tumours. Nature *490*, 61-70. 10.1038/nature11412.
21. Wiener, J.R., Kerns, B.J., Harvey, E.L., Conaway, M.R., Iglehart, J.D., Berchuck, A., and Bast, R.C., Jr. (1994). Overexpression of the protein tyrosine phosphatase PTP1B in human breast cancer: association with p185c-erbB-2 protein expression. J Natl Cancer Inst *86*, 372-378. 10.1093/jnci/86.5.372.
22. Banh, R.S., Iorio, C., Marcotte, R., Xu, Y., Cojocari, D., Rahman, A.A., Pawling, J., Zhang, W., Sinha, A., Rose, C.M., et al. (2016). PTP1B controls non-mitochondrial oxygen consumption by regulating RNF213 to promote tumour survival during hypoxia. Nat Cell Biol *18*, 803-813. 10.1038/ncb3376.
23. Kamada, F., Aoki, Y., Narisawa, A., Abe, Y., Komatsuzaki, S., Kikuchi, A., Kanno, J., Niihori, T., Ono, M., Ishii, N., et al. (2011). A genome-wide association study identifies RNF213 as the first Moyamoya disease gene. J Hum Genet *56*, 34-40. 10.1038/jhg.2010.132.
24. Nanba, R., Kuroda, S., Ishikawa, T., Iwasaki, Y., Tada, M., and Kiyohiro, H. (2004). [Familial moyamoya disease--clinical features and current study]. No Shinkei Geka *32*, 7-16.
25. Nanba, R., Kuroda, S., Tada, M., Ishikawa, T., Houkin, K., and Iwasaki, Y. (2006). Clinical features of familial moyamoya disease. Childs Nerv Syst *22*, 258-262. 10.1007/s00381-005-1230-5.
26. Ahel, J., Lehner, A., Vogel, A., Schleiffer, A., Meinhart, A., Haselbach, D., and Clausen, T. (2020). Moyamoya disease factor RNF213 is a giant E3 ligase with a dynein-like core and a distinct ubiquitin-transfer mechanism. Elife *9*. 10.7554/eLife.56185.

27. Bhardwaj, A., Banh, R.S., Zhang, W., Sidhu, S.S., and Neel, B.G. (2022). MMD-associated RNF213 SNPs encode dominant-negative alleles that globally impair ubiquitylation. Life Sci Alliance *5*. 10.26508/lsa.202000807.
28. Morito, D., Nishikawa, K., Hoseki, J., Kitamura, A., Kotani, Y., Kiso, K., Kinjo, M., Fujiyoshi, Y., and Nagata, K. (2014). Moyamoya disease-associated protein mysterin/RNF213 is a novel AAA+ ATPase, which dynamically changes its oligomeric state. Sci Rep *4*, 4442. 10.1038/srep04442.
29. Otten, E.G., Werner, E., Crespillo-Casado, A., Boyle, K.B., Dharamdasani, V., Pathe, C., Santhanam, B., and Randow, F. (2021). Ubiquitylation of lipopolysaccharide by RNF213 during bacterial infection. Nature *594*, 111-116. 10.1038/s41586-021-03566-4.
30. Takeda, M., Tezuka, T., Kim, M., Choi, J., Oichi, Y., Kobayashi, H., Harada, K.H., Mizushima, T., Taketani, S., Koizumi, A., and Youssefian, S. (2020). Moyamoya disease patient mutations in the RING domain of RNF213 reduce its ubiquitin ligase activity and enhance NFkappaB activation and apoptosis in an AAA+ domain-dependent manner. Biochem Biophys Res Commun *525*, 668-674. 10.1016/j.bbrc.2020.02.024.
31. Sugihara, M., Morito, D., Ainuki, S., Hirano, Y., Ogino, K., Kitamura, A., Hirata, H., and Nagata, K. (2019). The AAA+ ATPase/ubiquitin ligase mysterin stabilizes cytoplasmic lipid droplets. J Cell Biol *218*, 949-960. 10.1083/jcb.201712120.
32. Piccolis, M., Bond, L.M., Kampmann, M., Pulimeno, P., Chitraju, C., Jayson, C.B.K., Vaites, L.P., Boland, S., Lai, Z.W., Gabriel, K.R., et al. (2019). Probing the Global Cellular Responses to Lipotoxicity Caused by Saturated Fatty Acids. Mol Cell *74*, 32-44 e38. 10.1016/j.molcel.2019.01.036.
33. Habu, T., and Harada, K.H. (2021). UBC13 is an RNF213-associated E2 ubiquitin-conjugating enzyme, and Lysine 63-linked ubiquitination by the RNF213-UBC13 axis is responsible for angiogenic activity. FASEB Bioadv *3*, 243-258. 10.1096/fba.2019-00092.
34. Baumgartner, C.K., Paddock, M.N., Frost, J.M., Hamel, K.M., McGuire, K.A., Halliwill, K., Xiong, Z.M., Mu, L., Klinge, K., Geda, P., et al. (2022). ABBV-CLS-484: An active site PTPN2/N1 inhibitor that augments the immune response and sensitizes tumors to immune-mediated killing. Cancer Research *82*.
35. Branon, T.C., Bosch, J.A., Sanchez, A.D., Udeshi, N.D., Svinkina, T., Carr, S.A., Feldman, J.L., Perrimon, N., and Ting, A.Y. (2018). Efficient proximity labeling in living cells and organisms with TurboID. Nat Biotechnol *36*, 880-887. 10.1038/nbt.4201.
36. Teo, G., Liu, G., Zhang, J., Nesvizhskii, A.I., Gingras, A.C., and Choi, H. (2014). SAINTexpress: improvements and additional features in Significance Analysis of INTeractome software. J Proteomics *100*, 37-43. 10.1016/j.jprot.2013.10.023.
37. Kotani, Y., Morito, D., Sakata, K., Ainuki, S., Sugihara, M., Hatta, T., Iemura, S.I., Takashima, S., Natsume, T., and Nagata, K. (2017). Alternative exon skipping biases substrate preference of the deubiquitylase USP15 for mysterin/RNF213, the moyamoya disease susceptibility factor. Sci Rep *7*, 44293. 10.1038/srep44293.
38. Louvrier, C., Awad, F., Cosnes, A., El Khouri, E., Assrawi, E., Daskalopoulou, A., Copin, B., Bocquet, H., Chantot Bastaraud, S., Arenas Garcia, A., et al. (2022). RNF213-associated urticarial lesions with hypercytokinemia. J Allergy Clin Immunol *150*, 1545-1555. 10.1016/j.jaci.2022.06.016.

39. Ruzehaji, N., Kopecki, Z., Melville, E., Appleby, S.L., Bonder, C.S., Arkell, R.M., Fitridge, R., and Cowin, A.J. (2014). Attenuation of flightless I improves wound healing and enhances angiogenesis in a murine model of type 1 diabetes. Diabetologia *57*, 402-412. 10.1007/s00125-013-3107-6.
40. Bernatchez, P.N., Acevedo, L., Fernandez-Hernando, C., Murata, T., Chalouni, C., Kim, J., Erdjument-Bromage, H., Shah, V., Gratton, J.P., McNally, E.M., et al. (2007). Myoferlin regulates vascular endothelial growth factor receptor-2 stability and function. J Biol Chem *282*, 30745-30753. 10.1074/jbc.M704798200.
41. Roth Flach, R.J., Skoura, A., Matevossian, A., Danai, L.V., Zheng, W., Cortes, C., Bhattacharya, S.K., Aouadi, M., Hagan, N., Yawe, J.C., et al. (2015). Endothelial protein kinase MAP4K4 promotes vascular inflammation and atherosclerosis. Nat Commun *6*, 8995. 10.1038/ncomms9995.
42. Tamehiro, N., Zhou, S., Okuhira, K., Benita, Y., Brown, C.E., Zhuang, D.Z., Latz, E., Hornemann, T., von Eckardstein, A., Xavier, R.J., et al. (2008). SPTLC1 binds ABCA1 to negatively regulate trafficking and cholesterol efflux activity of the transporter. Biochemistry *47*, 6138-6147. 10.1021/bi800182t.
43. Chaurasia, B., and Summers, S.A. (2021). Ceramides in Metabolism: Key Lipotoxic Players. Annu Rev Physiol *83*, 303-330. 10.1146/annurev-physiol-031620-093815.
44. Chen, X., Huang, J., Yu, C., Liu, J., Gao, W., Li, J., Song, X., Zhou, Z., Li, C., Xie, Y., et al. (2022). A noncanonical function of EIF4E limits ALDH1B1 activity and increases susceptibility to ferroptosis. Nat Commun *13*, 6318. 10.1038/s41467-022-34096-w.
45. Kan, M.C., Oruganty-Das, A., Cooper-Morgan, A., Jin, G., Swanger, S.A., Bassell, G.J., Florman, H., van Leyen, K., and Richter, J.D. (2010). CPEB4 is a cell survival protein retained in the nucleus upon ischemia or endoplasmic reticulum calcium depletion. Mol Cell Biol *30*, 5658-5671. 10.1128/MCB.00716-10.
46. Roux, C.J., Barcia, G., Schiff, M., Sissler, M., Levy, R., Dangouloff-Ros, V., Desguerre, I., Edvardson, S., Elpeleg, O., Rotig, A., et al. (2021). Phenotypic diversity of brain MRI patterns in mitochondrial aminoacyl-tRNA synthetase mutations. Mol Genet Metab *133*, 222-229. 10.1016/j.ymgme.2021.04.004.
47. Rozman, D. (2000). Lanosterol 14alpha-demethylase (CYP51) - a cholesterol biosynthetic enzyme involved in production of meiosis activating sterols in oocytes and testis - a minireview. Pflugers Arch *439*, r056-r057. 10.1007/s004240000090.
48. Liu, W., Morito, D., Takashima, S., Mineharu, Y., Kobayashi, H., Hitomi, T., Hashikata, H., Matsuura, N., Yamazaki, S., Toyoda, A., et al. (2011). Identification of RNF213 as a susceptibility gene for moyamoya disease and its possible role in vascular development. PLoS One *6*, e22542. 10.1371/journal.pone.0022542.
49. Cecchi, A.C., Guo, D., Ren, Z., Flynn, K., Santos-Cortez, R.L., Leal, S.M., Wang, G.T., Regalado, E.S., Steinberg, G.K., Shendure, J., et al. (2014). RNF213 rare variants in an ethnically diverse population with Moyamoya disease. Stroke *45*, 3200-3207. 10.1161/STROKEAHA.114.006244.
50. Moquin, D.M., McQuade, T., and Chan, F.K. (2013). CYLD deubiquitinates RIP1 in the TNFalpha-induced necrosome to facilitate kinase activation and programmed necrosis. PLoS One *8*, e76841. 10.1371/journal.pone.0076841.

51. Kovalenko, A., Chable-Bessia, C., Cantarella, G., Israel, A., Wallach, D., and Courtois, G. (2003). The tumour suppressor CYLD negatively regulates NF-kappaB signalling by deubiquitination. Nature *424*, 801-805. 10.1038/nature01802.
52. Taniguchi, K., and Karin, M. (2018). NF-kappaB, inflammation, immunity and cancer: coming of age. Nat Rev Immunol *18*, 309-324. 10.1038/nri.2017.142.
53. Karki, R., and Kanneganti, T.D. (2019). Diverging inflammasome signals in tumorigenesis and potential targeting. Nat Rev Cancer *19*, 197-214. 10.1038/s41568-019-0123-y.
54. Menu, P., Mayor, A., Zhou, R., Tardivel, A., Ichijo, H., Mori, K., and Tschopp, J. (2012). ER stress activates the NLRP3 inflammasome via an UPR-independent pathway. Cell Death Dis *3*, e261. 10.1038/cddis.2011.132.
55. Dong, J., Miao, J., Miao, Y., Qu, Z., Zhang, S., Zhu, P., Wiede, F., Jassim, B.A., Bai, Y., Nguyen, Q., et al. (2023). Small Molecule Degraders of Protein Tyrosine Phosphatase 1B and T-Cell Protein Tyrosine Phosphatase for Cancer Immunotherapy. Angew Chem Int Ed Engl *62*, e202303818. 10.1002/anie.202303818.
56. Jura, N., Archer, H., and Bar-Sagi, D. (2005). Chronic pancreatitis, pancreatic adenocarcinoma and the black box in-between. Cell Res *15*, 72-77. 10.1038/sj.cr.7290269.
57. Grant, L., Shearer, K.D., Czopek, A., Lees, E.K., Owen, C., Agouni, A., Workman, J., Martin-Granados, C., Forrester, J.V., Wilson, H.M., et al. (2014). Myeloid-cell protein tyrosine phosphatase-1B deficiency in mice protects against high-fat diet and lipopolysaccharide-induced inflammation, hyperinsulinemia, and endotoxemia through an IL-10 STAT3-dependent mechanism. Diabetes *63*, 456-470. 10.2337/db13-0885.
58. Wiede, F., Lu, K.H., Du, X., Zeissig, M.N., Xu, R., Goh, P.K., Xirouchaki, C.E., Hogarth, S.J., Greatorex, S., Sek, K., et al. (2022). PTP1B Is an Intracellular Checkpoint that Limits T-cell and CAR T-cell Antitumor Immunity. Cancer Discov *12*, 752-773. 10.1158/2159-8290.CD-21-0694.
59. Medgyesi, D., Hobeika, E., Biesen, R., Kollert, F., Taddeo, A., Voll, R.E., Hiepe, F., and Reth, M. (2014). The protein tyrosine phosphatase PTP1B is a negative regulator of CD40 and BAFF-R signaling and controls B cell autoimmunity. J Exp Med *211*, 427-440. 10.1084/jem.20131196.
60. Stanford, S.M., and Bottini, N. (2023). Targeting protein phosphatases in cancer immunotherapy and autoimmune disorders. Nat Rev Drug Discov *22*, 273-294. 10.1038/s41573-022-00618-w.
61. Chen, X., Zeh, H.J., Kang, R., Kroemer, G., and Tang, D. (2021). Cell death in pancreatic cancer: from pathogenesis to therapy. Nat Rev Gastroenterol Hepatol *18*, 804-823. 10.1038/s41575-021-00486-6.
62. Scholz, C.C., Cavadas, M.A., Tambuwala, M.M., Hams, E., Rodriguez, J., von Kriegsheim, A., Cotter, P., Bruning, U., Fallon, P.G., Cheong, A., et al. (2013). Regulation of IL-1beta-induced NF-kappaB by hydroxylases links key hypoxic and inflammatory signaling pathways. Proc Natl Acad Sci U S A *110*, 18490-18495. 10.1073/pnas.1309718110.
63. An, J., Mo, D., Liu, H., Veena, M.S., Srivatsan, E.S., Massoumi, R., and Rettig, M.B. (2008). Inactivation of the CYLD deubiquitinase by HPV E6 mediates hypoxia-induced NF-kappaB activation. Cancer Cell *14*, 394-407. 10.1016/j.ccr.2008.10.007.

64. Thery, F., Martina, L., Asselman, C., Zhang, Y., Vessely, M., Repo, H., Sedeyn, K., Moschonas, G.D., Bredow, C., Teo, Q.W., et al. (2021). Ring finger protein 213 assembles into a sensor for ISGylated proteins with antimicrobial activity. Nat Commun *12*, 5772. 10.1038/s41467-021-26061-w.
65. Ohkubo, K., Sakai, Y., Inoue, H., Akamine, S., Ishizaki, Y., Matsushita, Y., Sanefuji, M., Torisu, H., Ihara, K., Sardiello, M., and Hara, T. (2015). Moyamoya disease susceptibility gene RNF213 links inflammatory and angiogenic signals in endothelial cells. Sci Rep *5*, 13191. 10.1038/srep13191.
66. Asselman, C., Hemelsoet, D., Eggermont, D., Dermaut, B., and Impens, F. (2022). Moyamoya disease emerging as an immune-related angiopathy. Trends Mol Med *28*, 939-950. 10.1016/j.molmed.2022.08.009.
67. Long, J., Sun, Y., Liu, S., Yang, S., Chen, C., Zhang, Z., Chu, S., Yang, Y., Pei, G., Lin, M., et al. (2023). Targeting pyroptosis as a preventive and therapeutic approach for stroke. Cell Death Discov *9*, 155. 10.1038/s41420-023-01440-y.
68. Wang, D., Wei, Y., and Pagliassotti, M.J. (2006). Saturated fatty acids promote endoplasmic reticulum stress and liver injury in rats with hepatic steatosis. Endocrinology *147*, 943-951. 10.1210/en.2005-0570.
69. Karasawa, T., Kawashima, A., Usui-Kawanishi, F., Watanabe, S., Kimura, H., Kamata, R., Shirasuna, K., Koyama, Y., Sato-Tomita, A., Matsuzaka, T., et al. (2018). Saturated Fatty Acids Undergo Intracellular Crystallization and Activate the NLRP3 Inflammasome in Macrophages. Arterioscler Thromb Vasc Biol *38*, 744-756. 10.1161/ATVBAHA.117.310581.
70. Marcotte, R., Sayad, A., Brown, K.R., Sanchez-Garcia, F., Reimand, J., Haider, M., Virtanen, C., Bradner, J.E., Bader, G.D., Mills, G.B., et al. (2016). Functional Genomic Landscape of Human Breast Cancer Drivers, Vulnerabilities, and Resistance. Cell *164*, 293-309. 10.1016/j.cell.2015.11.062.
71. Ran, F.A., Hsu, P.D., Wright, J., Agarwala, V., Scott, D.A., and Zhang, F. (2013). Genome engineering using the CRISPR-Cas9 system. Nat Protoc *8*, 2281-2308. 10.1038/nprot.2013.143.
72. Zhang, S., Iyer, S., Ran, H., Dolgalev, I., Gu, S., Wei, W., Foster, C.J.R., Loomis, C.A., Olvera, N., Dao, F., et al. (2021). Genetically Defined, Syngeneic Organoid Platform for Developing Combination Therapies for Ovarian Cancer. Cancer Discov *11*, 362-383. 10.1158/2159-8290.CD-20-0455.
73. Gibson, D.G., Young, L., Chuang, R.Y., Venter, J.C., Hutchison, C.A., 3rd, and Smith, H.O. (2009). Enzymatic assembly of DNA molecules up to several hundred kilobases. Nat Methods *6*, 343-345. 10.1038/nmeth.1318.

Figure 1

A

BT474	+	-	+	-	-	-	-
BT474 *RNF213*-KO	-	+	-	+	+	+	+
PTPN1-KD	-	-	+	+	+	+	+
+3x-FLAG-*RNF213*	-	-	-	-	-	+	-
+3x-FLAG-*RNF213*^{Y1275F}	-	-	-	-	-	-	+
+HA-*Ptp1b*$^{D/A}$	-	-	-	-	+	+	+

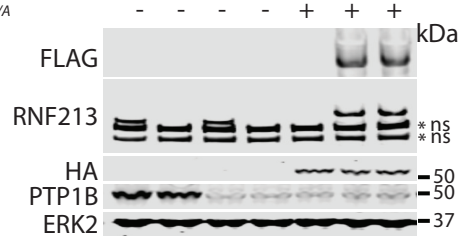

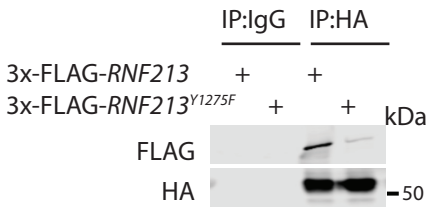

B

BT474 *RNF213*-KO-*PTPN1*-KD

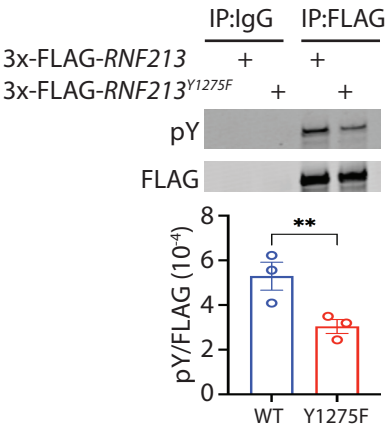

C

							IP:IgG	IP:FLAG	
BT474	+	-	+	-	-	-	-	-	-
BT474 *RNF213*-KO	-	+	-	+	+	+	+	+	+
PTPN1-KD	-	+	+	+	+	+	+	+	+
+3x-FLAG-*RNF213*	-	-	-	-	-	+	-	+	-
+3x-FLAG-*RNF213*^{Y1275F}	-	-	-	-	-	-	+	-	+
+*GFP-RNF213*	-	-	-	+	+	+	+	+	+

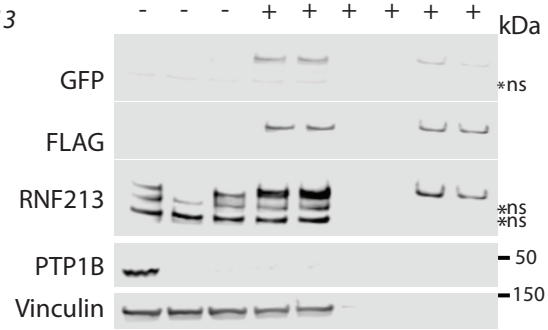

D

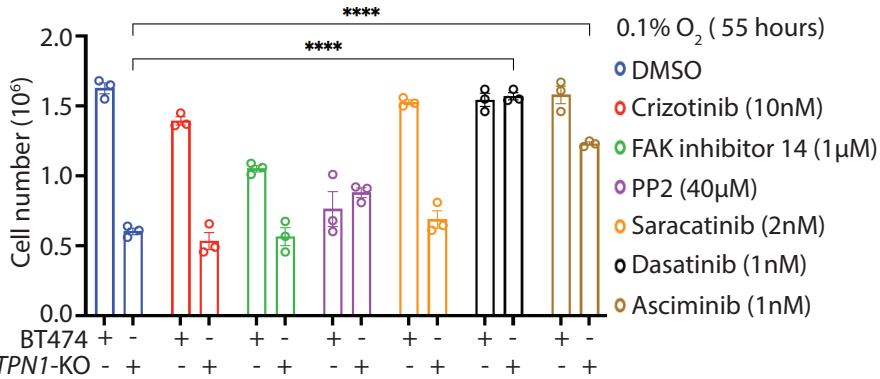

E

BT474	+	-	+	-	-	-	-
BT474 *RNF213*-KO	-	+	-	+	+	+	+
PTPN1-KD	-	-	+	+	+	+	+
+3x-FLAG-*RNF213*	-	-	-	-	-	+	+
+HA-*Ptp1b*$^{D/A}$	-	-	-	-	+	+	+
+Dasatinib (1 nM)	-	-	-	-	+	-	+

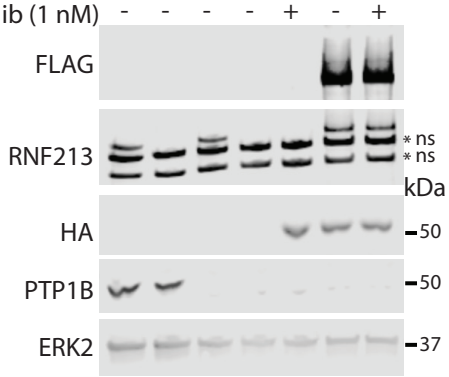

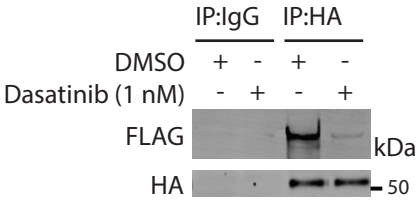

F

BT474 *RNF213*-KO-*PTPN1*-KD

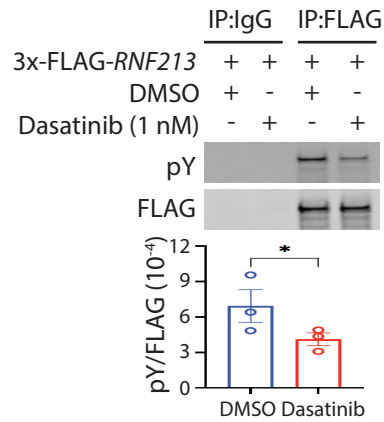

G

3x-FLAG-RNF213	-	-	+	-	+	+	+	+	-	-	-	-
3x-FLAG-RNF213^{Y1275F}	-	-	-	+	-	-	-	-	+	+	+	+
ABL1 (ng)	-	15	-	-	25	50	100	150	25	50	100	150

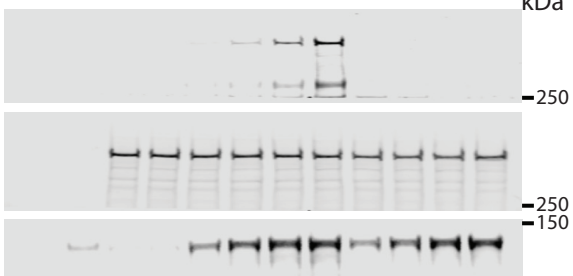

H

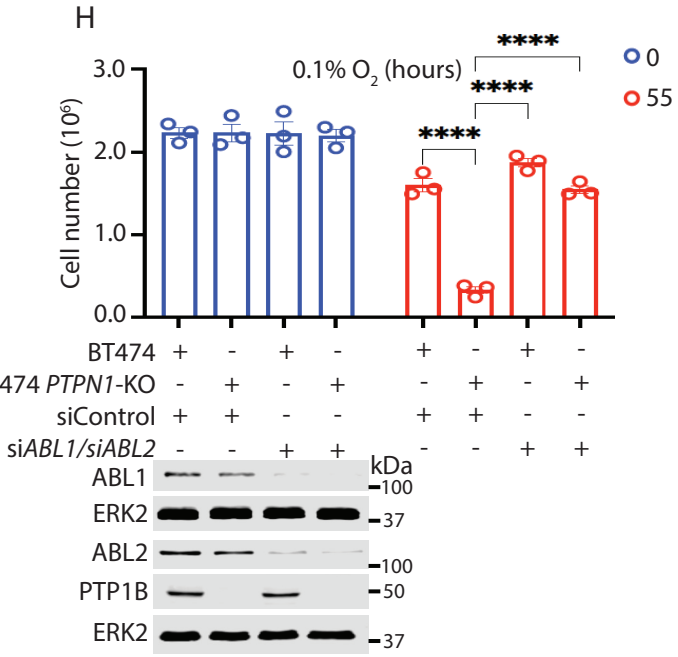

Figure 2

A

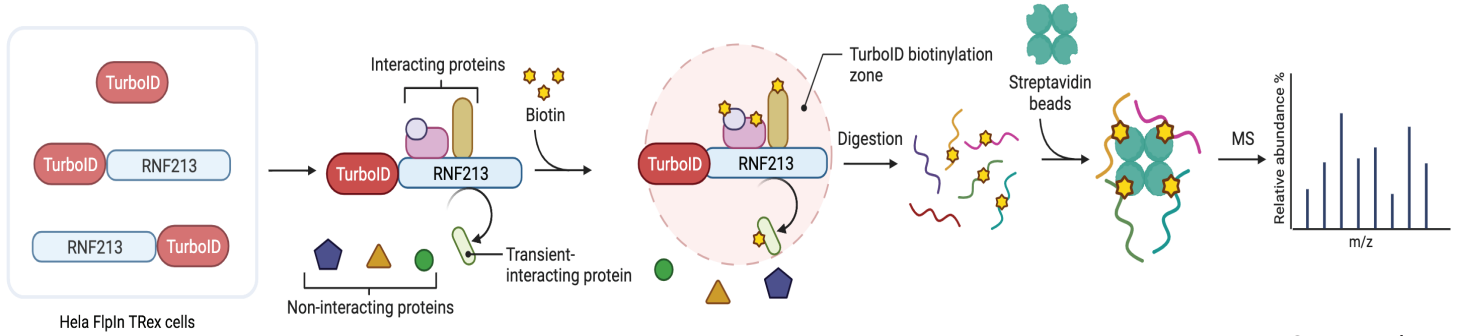

B

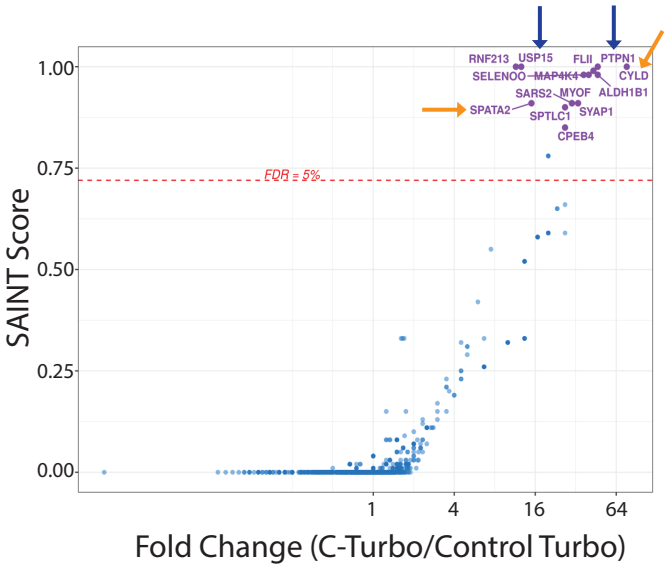

C

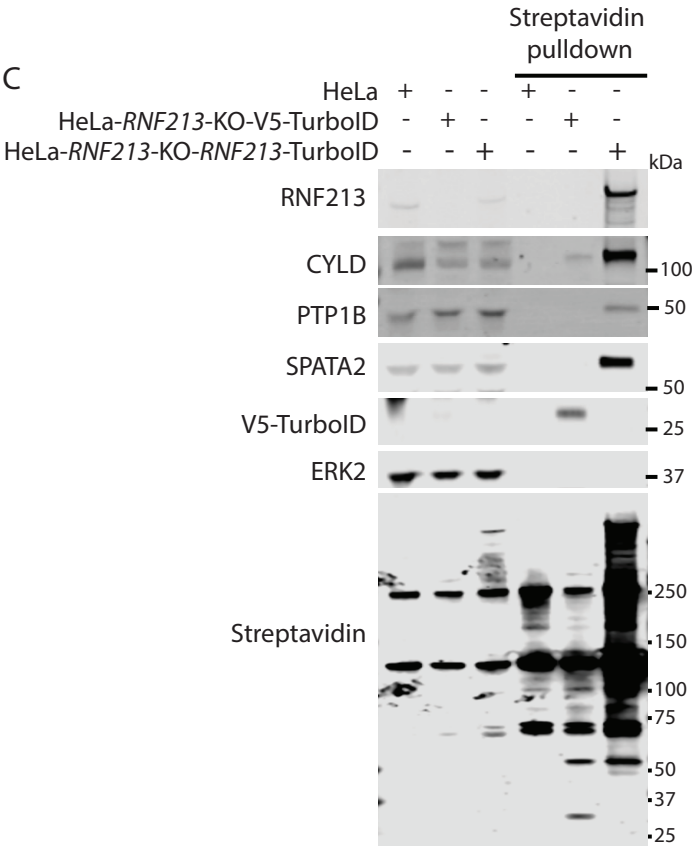

D

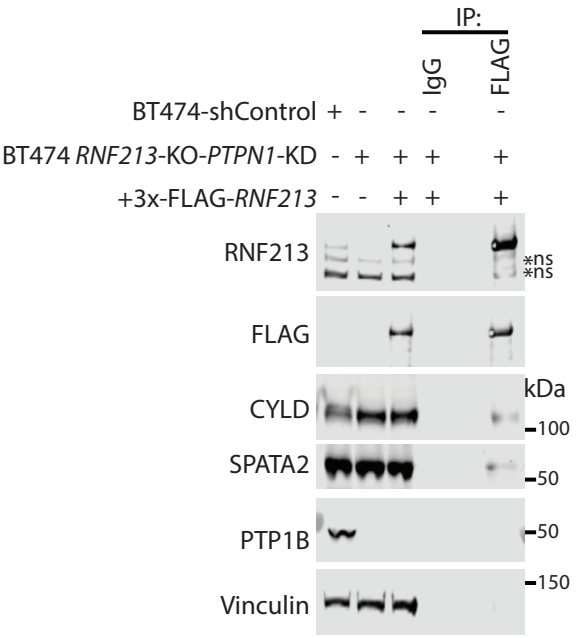

E

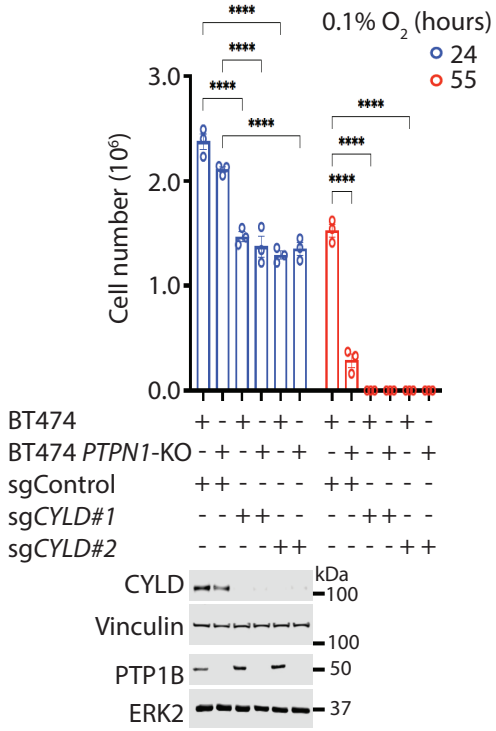

F

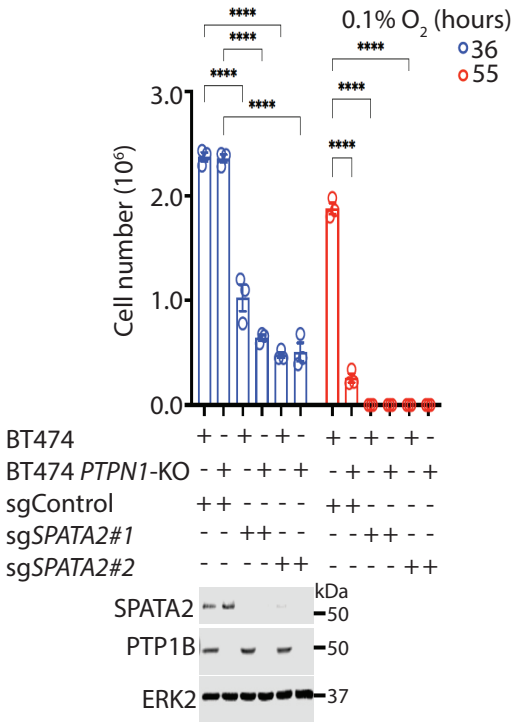

Figure 3

A

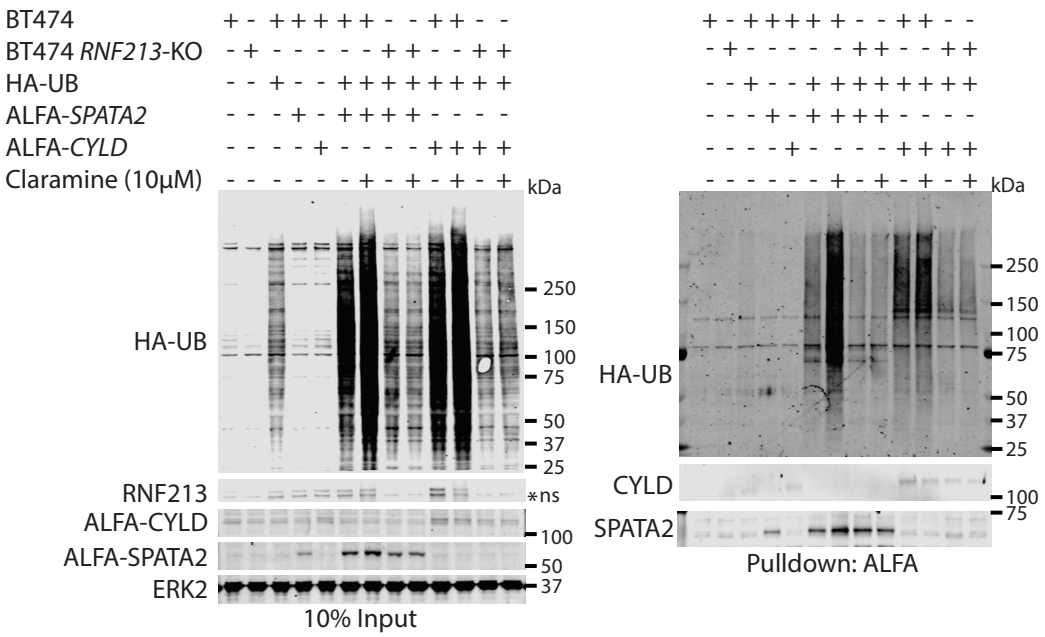

B

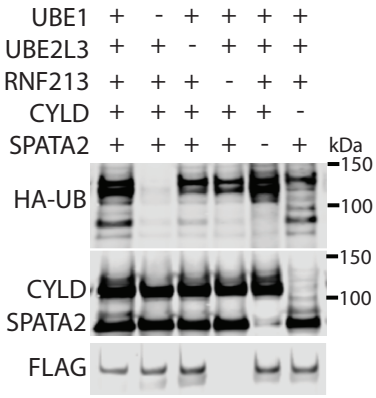

C

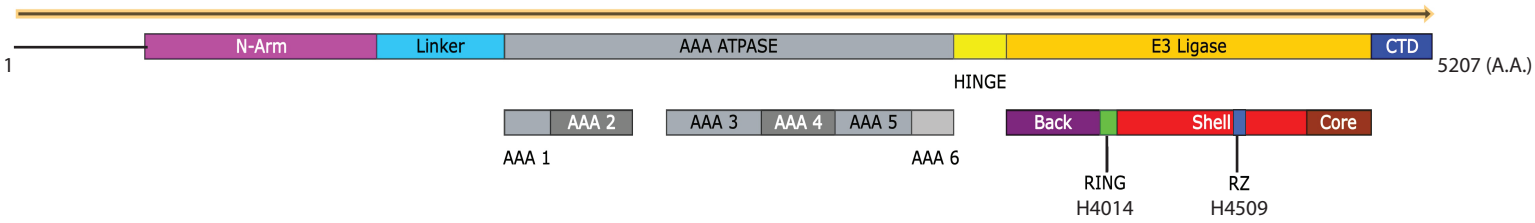

D

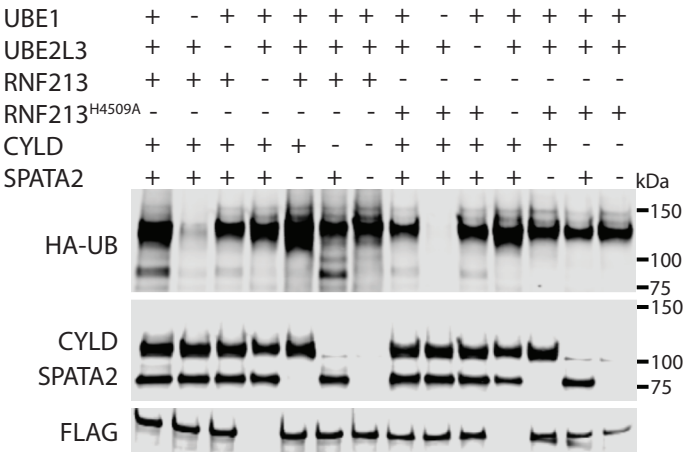

E

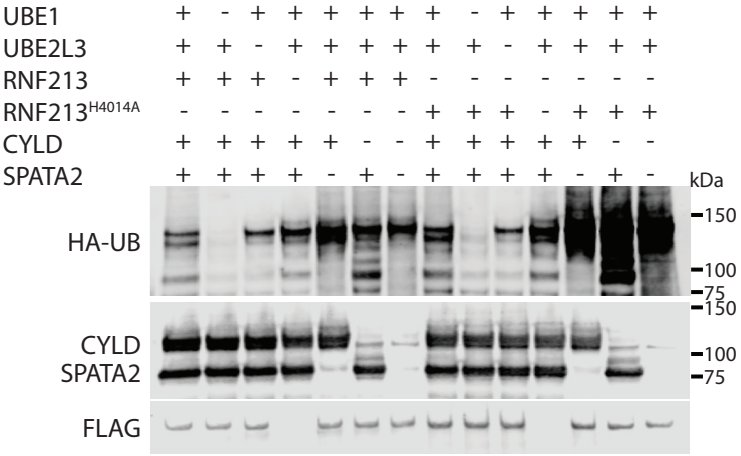

F

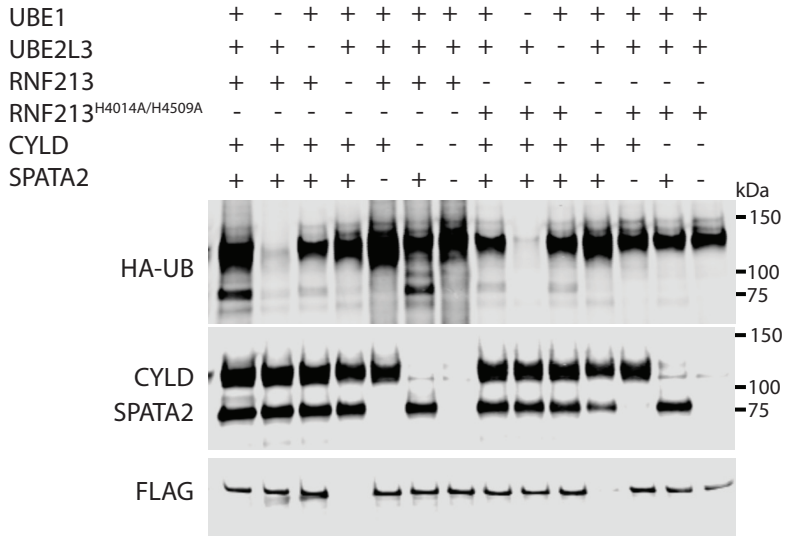

Figure 4

A

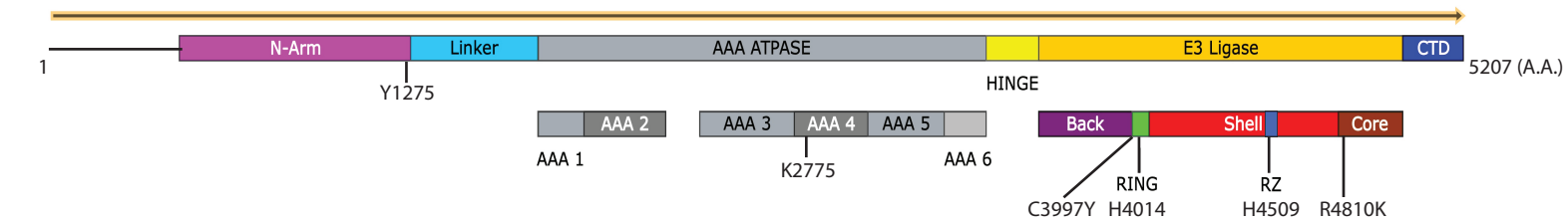

B

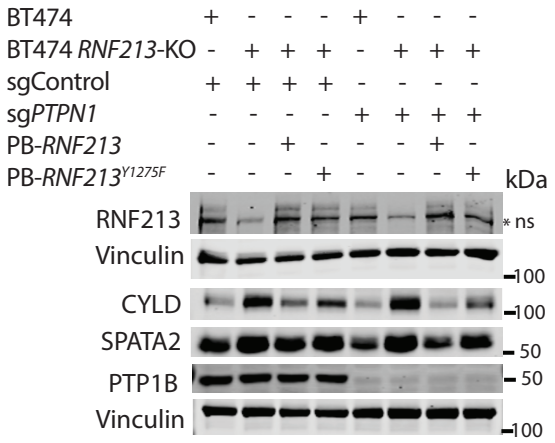

C

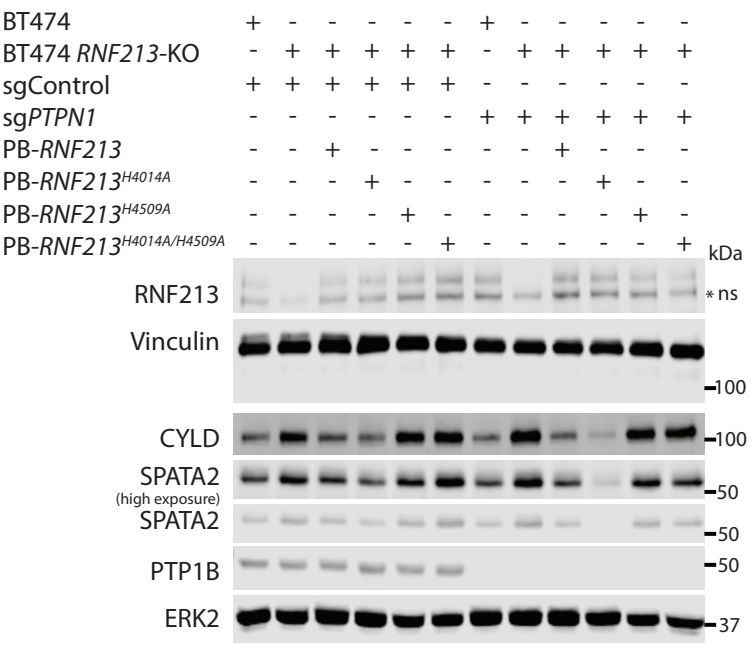

D

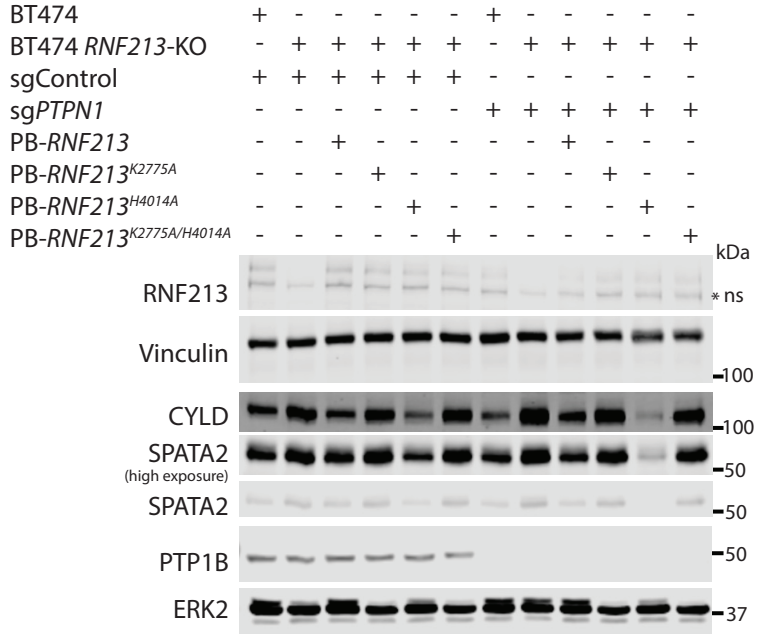

E

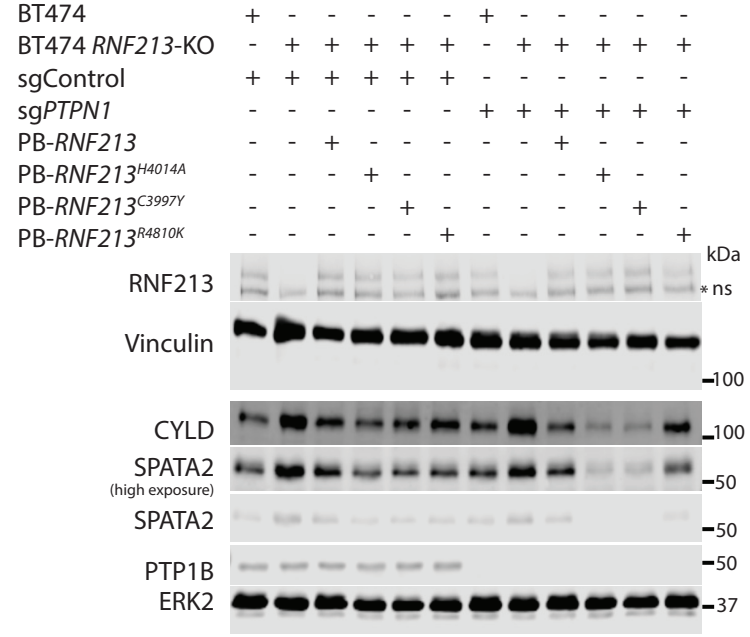

F

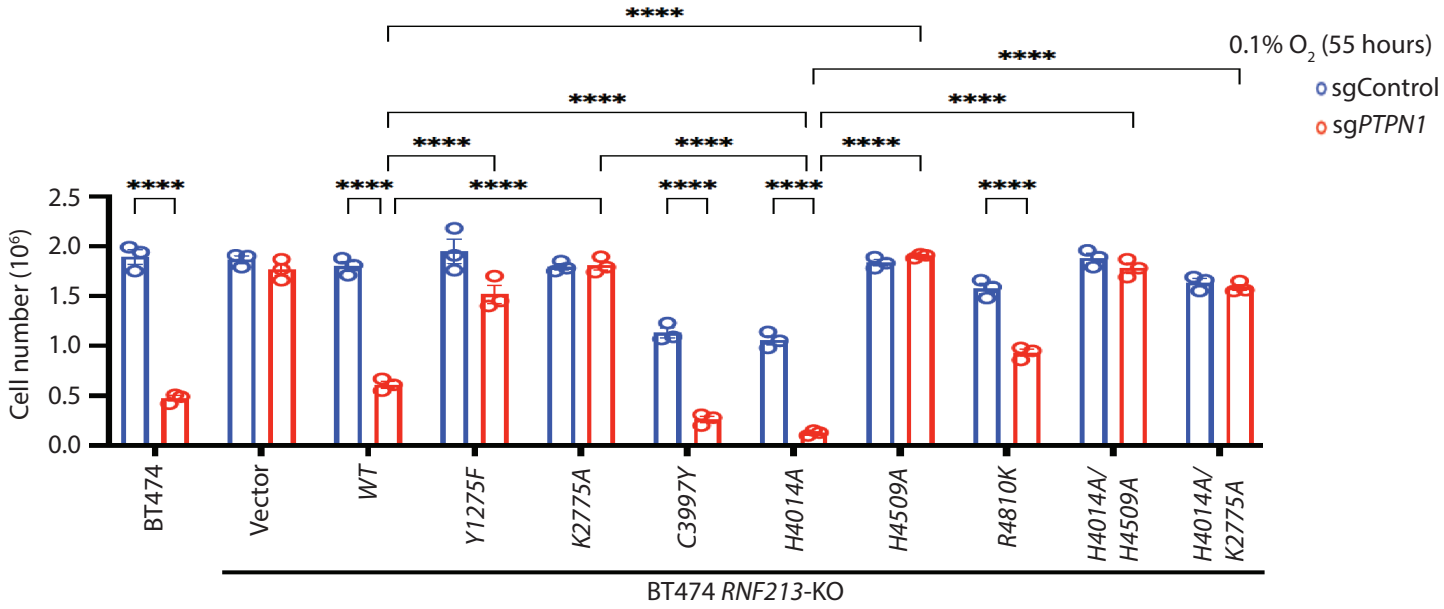

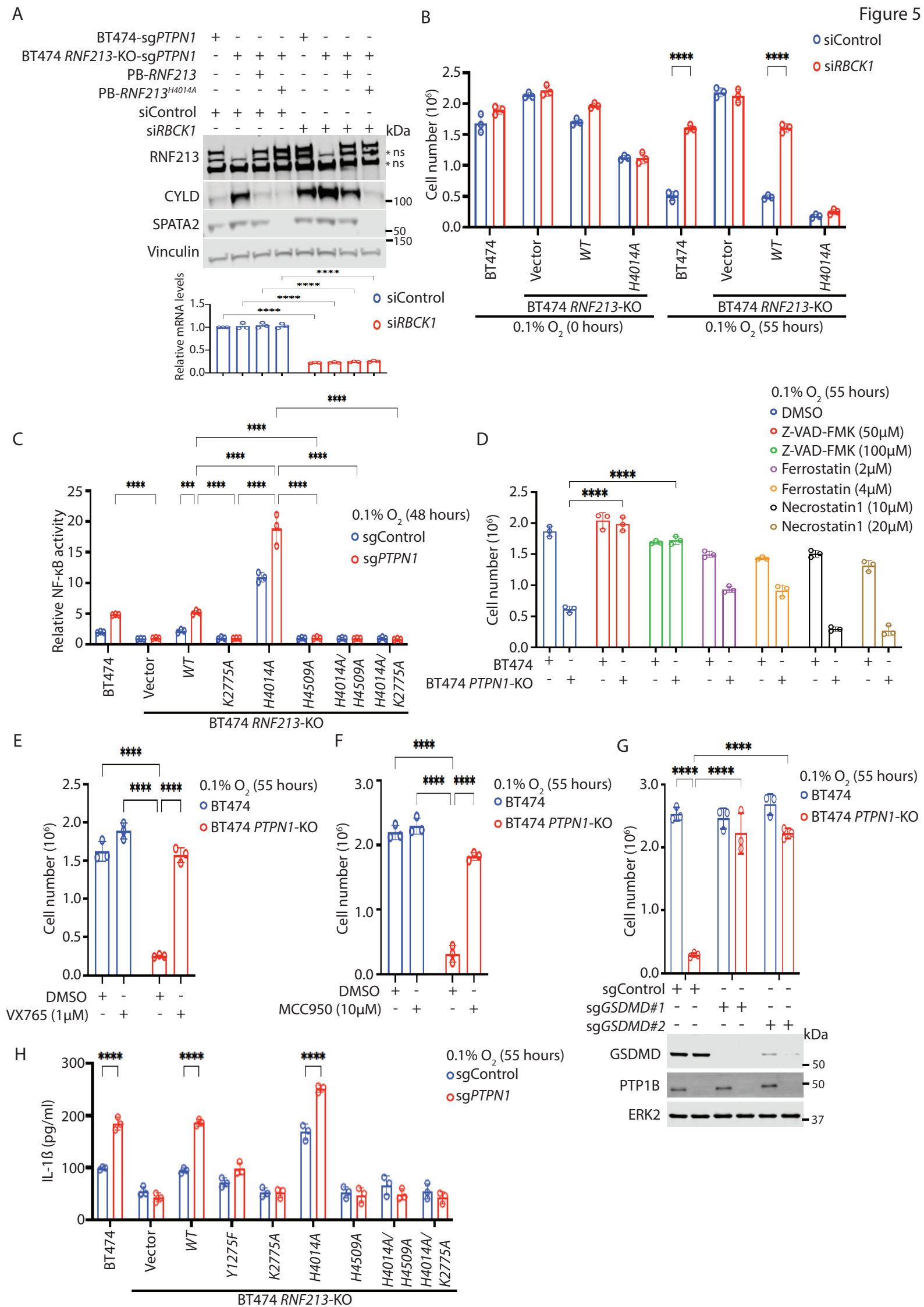
A
BT474-sgPTPN1
BT474 RNF213-KO-sgPTPN1
PB-RNF213
PB-RNF213H4014A
siControl
siRBCK1
kDa
RNF213
CYLD
SPATA2
Vinculin
* ns
* ns
100
50
150
Relative mRNA levels
siControl
siRBCK1
B
siControl
siRBCK1
Cell number (10^6)
BT474
Vector
WT
H4014A
BT474 RNF213-KO
0.1% O2 (0 hours)
0.1% O2 (55 hours)
C
Relative NF-κB activity
0.1% O2 (48 hours)
sgControl
sgPTPN1
BT474
Vector
WT
K2775A
H4014A
H4509A
H4014A/H4509A
H4014A/K2775A
BT474 RNF213-KO
D
0.1% O2 (55 hours)
DMSO
Z-VAD-FMK (50μM)
Z-VAD-FMK (100μM)
Ferrostatin (2μM)
Ferrostatin (4μM)
Necrostatin1 (10μM)
Necrostatin1 (20μM)
Cell number (10^6)
BT474
BT474 PTPN1-KO
E
Cell number (10^6)
0.1% O2 (55 hours)
BT474
BT474 PTPN1-KO
DMSO
VX765 (1μM)
F
Cell number (10^6)
0.1% O2 (55 hours)
BT474
BT474 PTPN1-KO
DMSO
MCC950 (10μM)
G
Cell number (10^6)
0.1% O2 (55 hours)
BT474
BT474 PTPN1-KO
sgControl
sgGSDMD#1
sgGSDMD#2
kDa
GSDMD
PTP1B
ERK2
50
50
37
H
IL-1ß (pg/ml)
0.1% O2 (55 hours)
sgControl
sgPTPN1
BT474
Vector
WT
Y1275F
K2775A
H4014A
H4509A
H4014A/H4509A
H4014A/K2775A
BT474 RNF213-KO

A

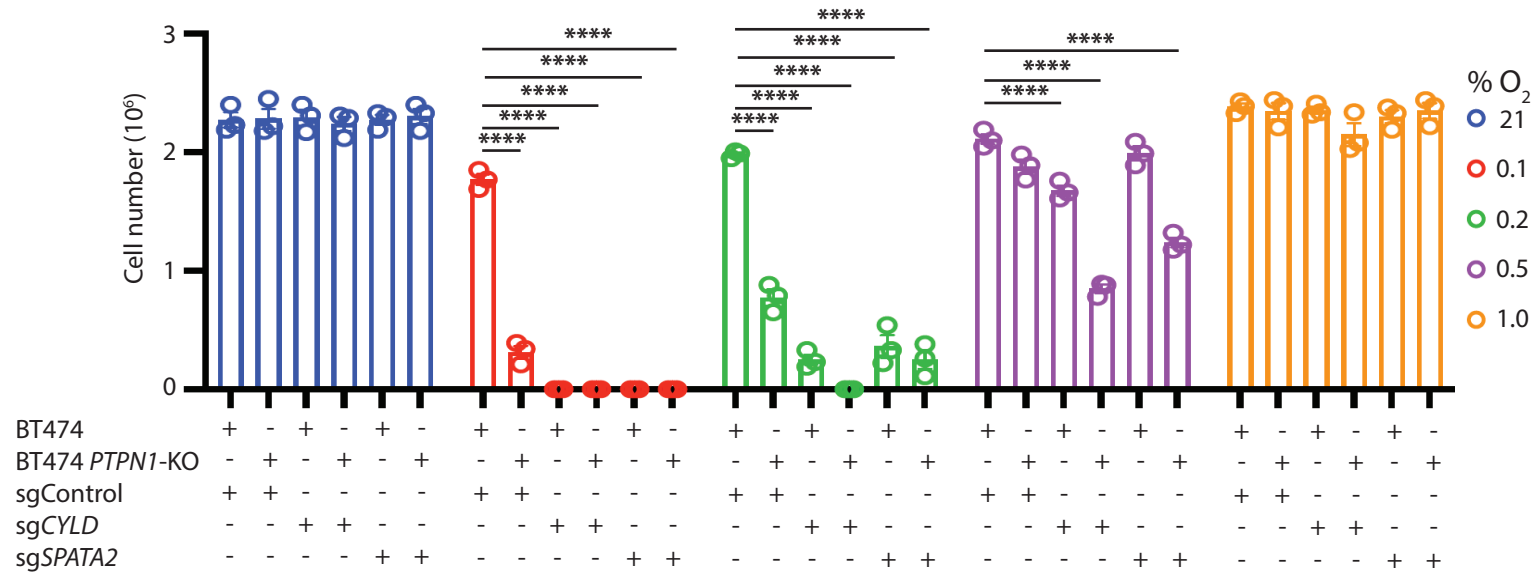
Cell number (10⁶)
% O2
21
0.1
0.2
0.5
1.0
BT474
BT474 PTPN1-KO
sgControl
sgCYLD
sgSPATA2

B

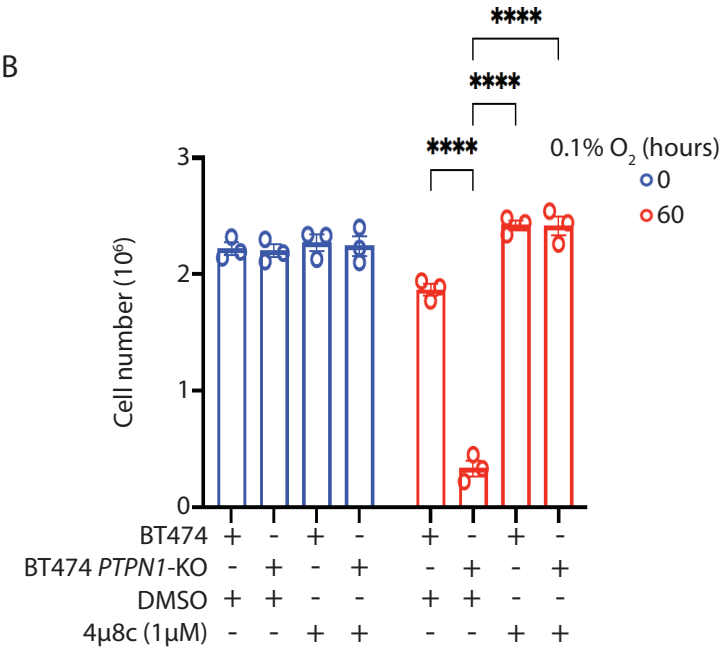
Cell number (10⁶)
0.1% O2 (hours)
0
60
BT474
BT474 PTPN1-KO
DMSO
4μ8c (1μM)

C

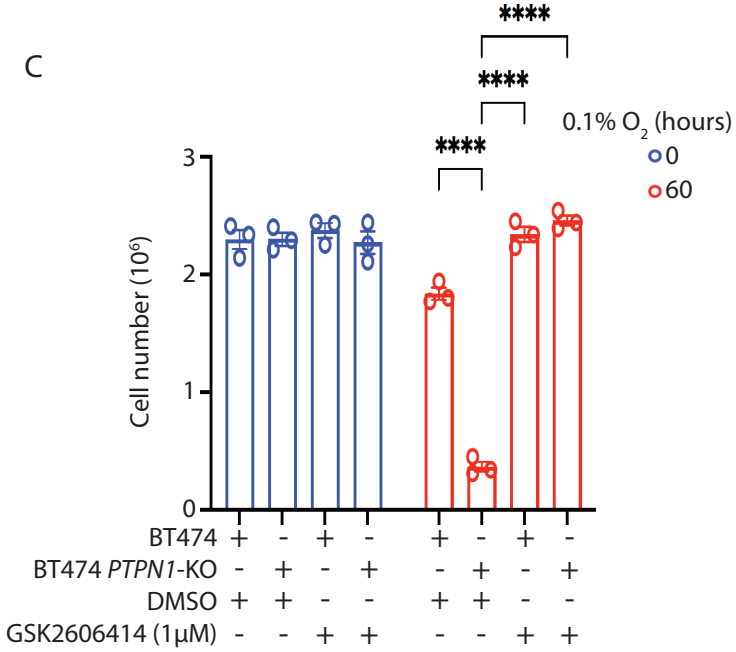
Cell number (10⁶)
0.1% O2 (hours)
0
60
BT474
BT474 PTPN1-KO
DMSO
GSK2606414 (1μM)

D

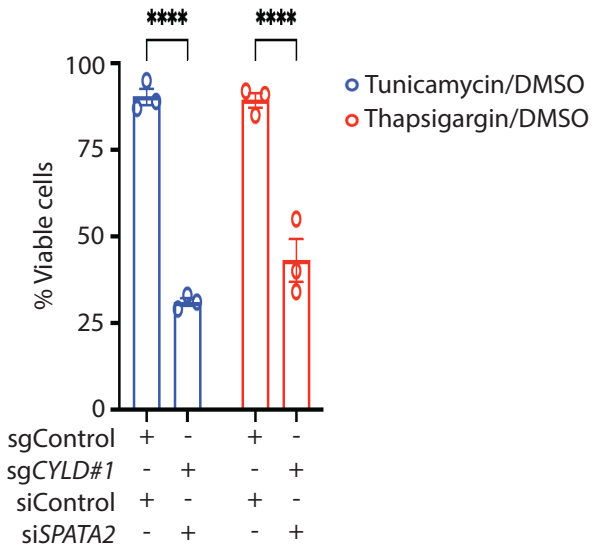
% Viable cells
Tunicamycin/DMSO
Thapsigargin/DMSO
sgControl
sgCYLD#1
siControl
siSPATA2

Figure 7

A

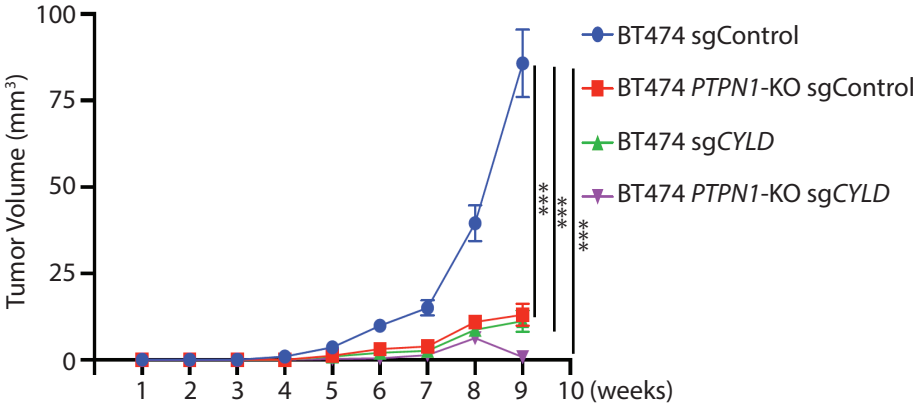

B

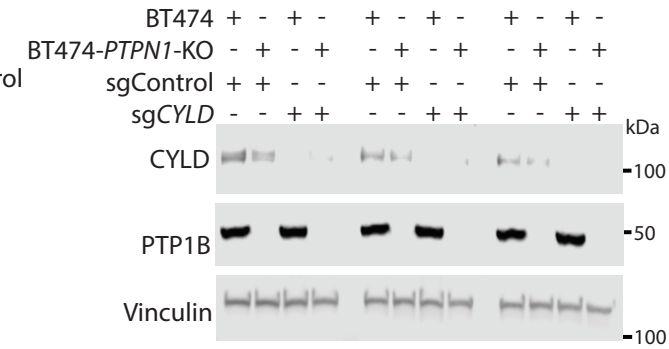

C

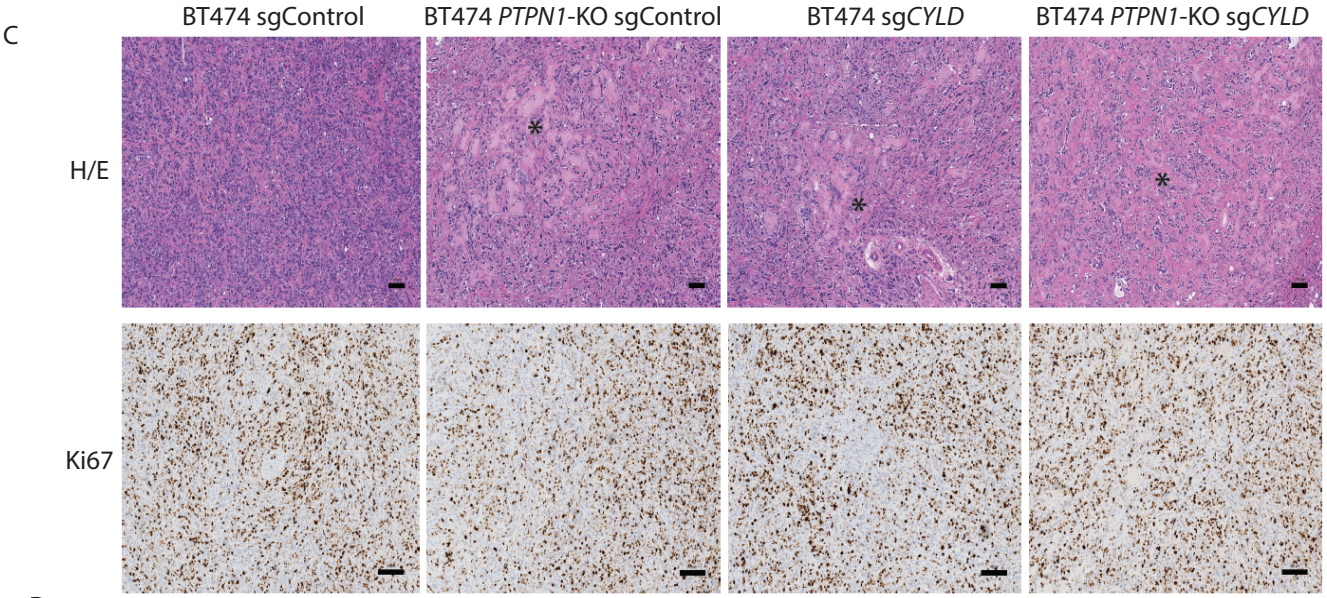
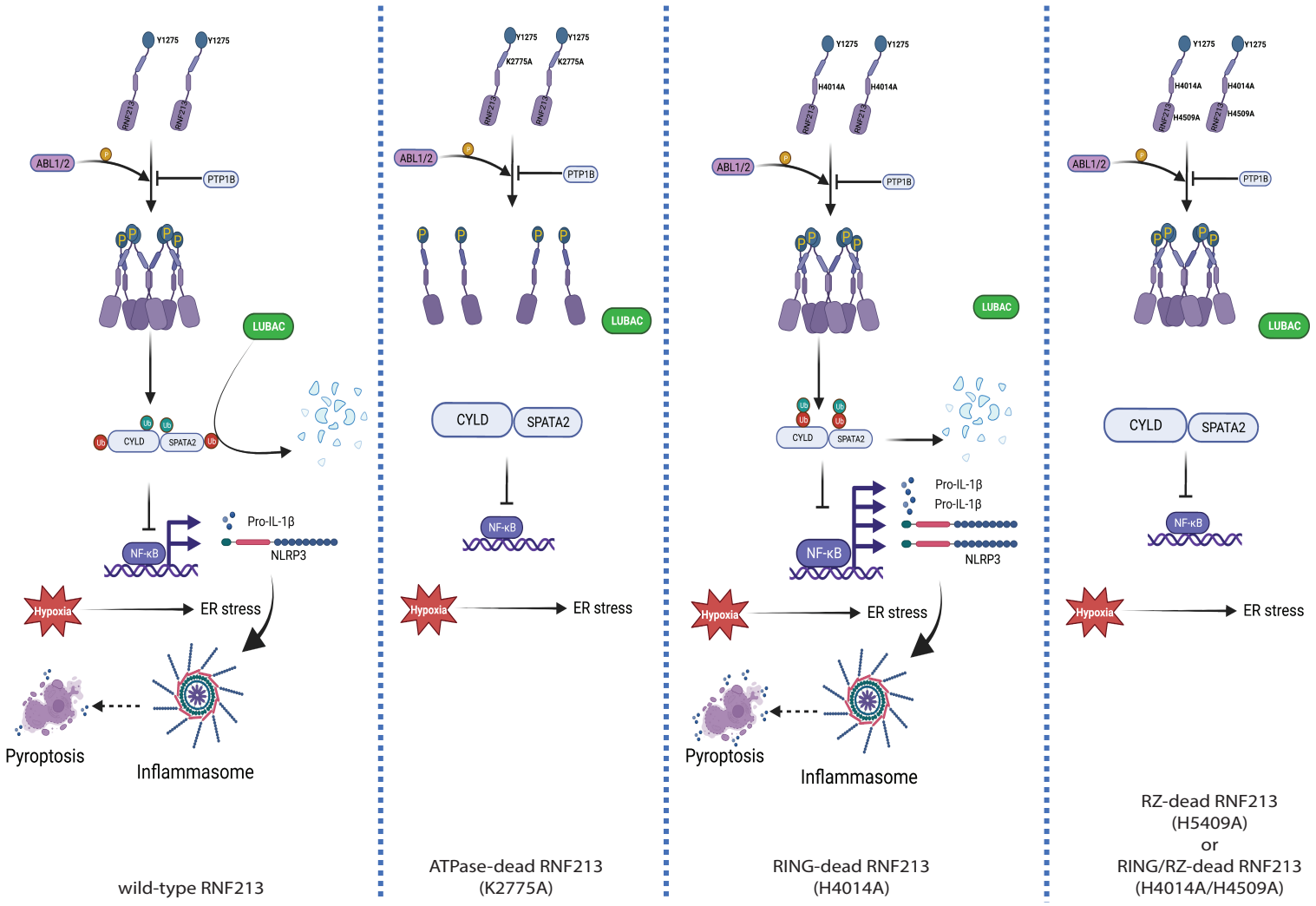
D